UNIVERSITÀ
DEGLI STUDI
DI PADOVA

Sede Amministrativa: Università degli Studi di Padova

Dipartimento di Medicina Molecolare

CORSO DI DOTTORATO DI RICERCA IN: Medicina Molecolare
CURRICULUM: Biomedicina
CICLO XXXII

Unraveling the mechanism of ferroptosis

Coordinatore: Ch.mo Prof. Stefano Piccolo
Supervisore: Ch.mo Prof. Fulvio Ursini
Co-Supervisore: Ch.ma Dott.ssa Antonella Roveri

Dottoranda: Ana-Marija Vučković

ABSTRACT

Ferroptosis, a form of regulated cell death (RCD), has been recently reported to be primed by missing activity of the ubiquitous selenoperoxidase glutathione peroxidase 4 (GPx4). GPx4 catalyzes a glutathione (GSH)-dependent reduction of membrane hydroperoxides to corresponding alcohols. Since ferroptosis is executed by lipid peroxidation, oxygen, polyunsaturated fatty acids (PUFA), and iron are necessary constraints. Furthermore, since phospholipid hydroperoxides (PL-OOH) have a key role in membrane lipid peroxidation –i.e. their decomposition generates radicals in the membranes- GPx4-mediated regulation of ferroptosis is consistent with both, the mechanisms of lipid peroxidation and protection which have been finely elucidated *in vitro* in the last forty years of the XX century.

In this study, we used as a suitable model of ferroptotic cell death, that primed by erastin in HT1080 cells. Erastin, by preventing cystine import, in these cells decreases the cellular level of GSH and, consequently, GPx4 activity. On this model, we disclosed a critical constraint permitting membrane lipid oxidation and therefore ferroptosis execution. Unexpectedly, we observed that modulating the electron flow through the mitochondria respiratory chain, is indeed unsuccessful in modulating ferroptosis sensitivity. For this indispensable function we identified, instead, the activity of mitochondrial α-keto acid dehydrogenases. The deduced mechanism we propose is the formation of $O_2^{\bullet-}$ during re-oxidation of dihydrolipoate in the last step of the oxidative decarboxylation, a reaction, already observed in isolated mitochondria. In relation to ferroptosis, we propose that it is the $HO_2^{\bullet}$ that generates a carbon centered radical in a PUFA, which, following oxygen addiction and stabilization by hydrogen transfer, forms a PL-OOH.

We also studied the mechanisms underlying the inhibition of GPx4 by a prototype of electrophile: (1*S*,3*R*) RSL3. This study allowed to disclose the protein 14-3-3ε as an adaptor protein necessary to achieve GPx4 inactivation by (1*S*,3*R*) RSL3. By these observations, we clarified the requirements for GPx4 inactivation by electrophiles, which, *in vivo* is supposed to have a regulatory role. Further, we provided evidence that the 'inactivation-permitting activity' of 14-3-3ε on GPx4 is redox regulated by thiol-disulphide transition. This links inhibition by electrophiles to intracellular redox status.

This set of new information contributes to the view of cell death by ferroptosis as intrinsically connected to aerobic life through a fine modulation of specific metabolic events. It is an amazing thought that electron transitions between oxygen and iron permits in aerobic organism both, life and death. The latter, therefore, comes up as a fundamental component of aerobic life.

RIASSUNTO

La ferroptosi, una forma di morte cellulare regolata (RCD) è stata recentemente descritta essere innescata dalla mancata attività della selenoperossidasi ubiquitaria glutatione perossidasi 4 (GPx4). La GPx4 catalizza la riduzione glutatione (GSH)-dipendente degli idroperossidi di membrana ad alcoli corrispondenti. Essendo conseguenza di perossidazione lipidica, elementi vincolanti la ferroptosi sono ossigeno, acidi grassi polinsaturi (PUFA) e ferro. Inoltre, avendo i perossidi dei fosfolipidi (PL-OOH) un ruolo chiave nella perossidazione lipidica di membrana -la loro decomposizione comporta infatti la formazione di radicali nelle membrane-, la regolazione della ferroptosi da parte della GPx4 è consistente sia con i meccanismi di perossidazione lipidica che con quelli di protezione, entrambi finemente elucidati *in vitro* nell'ultimo quarantennio del XX secolo.

In questo studio, abbiamo usato come modello di ferroptosi il trattamento con erastina di cellule HT1080. Prevenendo l'importazione di cistina, in queste cellule, l'erastina riduce i livelli di GSH intracellulare e quindi l'attività GPx4. Su questo modello, il nostro studio ha rivelato uno dei possibili elementi critici che innescano l'ossidazione dei lipidi di membrana e quindi l'esecuzione della ferroptosi. Abbiamo infatti osservato inaspettatamente che la modulazione del flusso di elettroni nella catena respiratoria dei mitocondri, riconosciuta modulare i livelli di anione superossido ($O_2^{\bullet-}$) e della sua forma protonata, la specie pro-ossidante $HO_2^{\bullet}$, non influisce sulla sensibilità alla ferroptosi. Per questa funzione indispensabile abbiamo invece identificato l'attività delle α-cheto acido deidrogenasi mitocondriali. Il meccanismo che proponiamo è la formazione di $O_2^{\bullet-}$ durante la riossidazione del diidrolipoato nell'ultima fase della reazione di decarbossilazione ossidativa, una reazione già osservata nei mitocondri isolati. In relazione alla ferroptosi, proponiamo che sia la forma $HO_2^{\bullet}$ a generare un radicale sul carbonio metilenico di un acido grasso polinsaturo (PUFA) di un fosfolipide di membrana. Questo, in seguito all'aggiunta di ossigeno e alla stabilizzazione mediante trasferimento di idrogeno, formerebbe un fosfolipide idroperossido (PL-OOH).

Abbiamo inoltre studiato il meccanismo di inibizione della GPx4 da parte di un prototipo di elettrofilo: (1*S*,3*R*) RSL3. Questo studio ha permesso l'identificazione della proteina 14-3-3ε, come la proteina adattatrice necessaria per l'inattivazione della GPx4 da parte di (1*S*,3*R*) RSL3. Sono stati così chiariti i requisiti per l'inattivazione da elettrofili della GPx4, che probabilmente, *in vivo*, ha un significato regolatorio. Abbiamo inoltre fornito prove sul fatto che l'attività che permette l'inattivazione di GPx4 della 14-3-3ε è regolata redox da transizioni tiolo - disolfuro, legando quindi la capacità inibitoria degli elettrofili allo stato redox intracellulare.

Questa serie di informazioni contribuisce alla visione della morte cellulare per ferroptosi come un fenomeno intrinsecamente connesso alla vita aerobica attraverso la fine modulazione di specifici eventi metabolici. Invero, risulta sorprendente pensare che le transizioni di elettroni tra ossigeno e ferro consentano agli organismi aerobici sia la vita che la morte, facendo emergere quest'ultima come una componente fondamentale della stessa vita aerobia.

INDEX

1. INTRODUCTION

1.1 History of cell death research

The term "cell death" describes an ultimate failure of cell to maintain homeostatic processes supporting life. The research on naturally occurring cell death started already in 19th century when Carl Vogt made his first observation of physiological cell death occurring during normal development of metamorphic toads[1]. However, the concept remained mainly forgotten until the beginning of 1960s when it was noticed that cell death occurring during development is biologically controlled[2]. These observations helped to establish the concept of "programmed cell death". We now understand that programmed cell death is indispensable for tissue homeostasis and normal development, and, when unregulated, contributes to pathological conditions.

As cell death manifests with various morphological alternations, in 1970s scientists started to categorize cell death modalities based on morphological features. Cell death was first classified into three different classes: i) type I manifesting chromatin condensation and nuclear fragmentation of cells undergoing phagocytosis, taken up and degraded in lysosomes by neighbouring cells ii) type II exhibiting cytoplasmatic vacuolization in dying cells, similarly activating phagocytosis and lysosomal degradation iii) type III cell death associated with fragmentation without phagocytic and lysosomal involvement[3,4]. For decades this classification was adopted to describe cell death types we know today as apoptosis, autophagy and necrosis, respectively.

A huge breakthrough in the field of cell death research was made in 1972 by John Kerr and colleagues when they first used the term of apoptosis (from Greek – falling off) in order to distinguish developmental programmed cell death from accidental cell death - necrosis[5]. In their historical paper it was demonstrated that cells undergoing apoptosis in contrast to necrosis manifest specific morphological alternations. However, unification of the process of "programmed cell death" in invertebrates with "apoptosis" in vertebrates did not happen until the 90's when the development of modern techniques allowed a genetic understanding of programmed cell death[6]. Genetic studies performed in the model of *Caenorhabditis elegans* identified the requirement of specific genes to induce cell death during development[7]. This observation definitely stated that programmed cell death is a well-conserved, genetically regulated cellular process.

1.2 The concept of regulated cell death

The term regulated describes a cell death mechanism that requires a genetically encoded machinery operating a sequence of specific events that eventually kill the cell[8]. It is important to note that even though programmed and regulated cell death (RCD) might display some similar features, these two terms represent two different settings of non-accidental death[4]. In other words, RCD can occur in two different scenarios: (I) in a physiological setting known as programmed cell death involved in development and tissue homeostasis, which originate in absence of any exogenous perturbation; (II) as a result of perturbations of the intracellular or extracellular environment, carried out by specific genetically encoded molecular mechanisms[9]. Thus, programmed cell death can be considered as a subclass of RCD.

Apoptosis is the best characterized form of programmed cell death that involves the activation of a family of cysteine proteases, also called caspases[10]. It can be initiated by an extrinsic or intrinsic death-inducing signalling pathway, both terminating by the activation of caspase 3 and caspase 7. Briefly, the intrinsic pathway is controlled by anti-apoptotic proteins like B-cell lymphoma 2 (BCL-2), BCL-extra-large (BCL-XL) and myeloid leukemia cell differentiation 1 (MCL1) whose degradation or inhibition leads to disruption of the outer mitochondrial membrane and release of cytochrome c[11–13]. Cytochrome c forms a complex with apoptotic protease-activating factor 1 (APAF1) which activates caspase 3 and 7 by cleavage[14]. The extrinsic pathway, instead, is initiated by extracellular ligands binding to cell death receptors and leading to the formation of the death-inducing signalling complexes (DISC)[15]. DISC activates caspase 8 which further activates caspase 3 and 7. In both scenarios, caspases cleave a variety of protein substrates leading to loss-of-function of truncated proteins and disruption of essential cellular processes.

For decades apoptosis was considered as a synonym for RCD, while necrosis indicated cell death in general, not genetically controlled and occurring in response to physical or chemical insults. However, the notion that also necrosis can be biochemically regulated arises in 1980s and it took almost 20 years before necroptosis (a neologism introduced in analogy to apoptosis) was recognized as a specific form of RCD[16,17]. Genetic evidences and discoveries of necroptosis inhibitors confirmed an involvement of a peculiar, caspase-independent, molecular machinery encompassing specific receptor interacting protein kinases (RIP1 and RIP3) and death receptors[18–20]. It was demonstrated that necroptosis participates in the maintenance of adult T-cell homeostasis and in developmental programmes thus supporting the classification as programmed cell death[4,21].

The field of cell death research continues to grow from discoveries about the causative role in various pathological conditions. In addition, the regulative nature of certain cell death forms is compatible with pharmacological modulation and the development of innovative targeted therapy[22].

Thus, along with apoptosis and necroptosis, newly discovered RCD pathways were proposed and gained increasing consideration, such as pyroptosis, parthanatos, NETosis and ferroptosis, each named after the specific feature of cell death they represent. As an increasing number of novel signalling pathways that orchestrate RCD are still being defined, in 2012 Nomenclature Committee of Cell Death (NCCD) recommended replacing the morphologic classification of cell death subroutines with a new classification grounded on molecular events and biochemical features[23].

In my dissertation I will focus on ferroptosis, a recently discovered RCD pathway and whose mechanisms do not overlap with other cell death modalities.

Ferroptosis is a newly form of RCD initiated by oxidative perturbations of the intracellular microenvironment primed by missing or insufficient activity of glutathione peroxidase 4 (GPx4)[24]. Ferroptosis is axiomatically associated with membrane lipid peroxidation that is the oxidative degradation of polyunsaturated fatty acyl in phospholipids initiated by addition of molecular di-oxygen (O_2). The first description of lipid peroxidation of biological membranes was proposed more than 60 years ago, but only recently these reactions are seen as biologically regulated events impacting on cell life and death[25].
Lipid peroxidation emerged as the executor of ferroptosis from studies using lethal molecules that either deplete the substrate of GPx4, glutathione (GSH), or directly inhibit GPx4[26,27]. GPx4 negatively regulates ferroptosis owing its capacity to reduce phospholipid hydroperoxides (PL-OOH) into corresponding alcohols (PL-OH) using two molecules of GSH[28]. Thus, ferroptosis is only initiated when GPx4 activity is not sufficient to cope with PL-OOH normally produced by cellular processes. In such a way ferroptosis cannot be seen as an outcome of a pathway initiated by a specific agonist but rather as an outcome of insufficient enzymatic control of lipid peroxidation.

1.2.1.Ferroptosis, a new form of regulated cell death

The term of ferroptosis (from Latin “ferrum”- iron and Greek “ptosis”- fall) was coined in 2012 by Dixon in the B. R. Stockwell Lab to describe a RCD pathway defined as a result of missing GPx4, which was assumed to be associated to lipid peroxidation[24,27]. In this respect it is worth noting that it is on the already well known anti-peroxidant activity of GPx4 that the crucial role of lipid peroxidation in ferroptosis was originally proposed. During ferroptosis the level of lipid peroxidation is extremely low and extremely difficult to quantify, and it is for this reason that just the oxidation of BODIPY C11 –a redox sensitive fluorescent probe- is almost invariably adopted in studies on ferroptosis as an index of on-going peroxidation.

Originally, the term ferroptosis first used to characterize the peculiar features of cell death induced by either RAS selective lethal 3 (RSL3) molecule or a small molecule erastin able to eradicate RAS- and Small Transformed cells discovered in synthetic lethal screening using small molecule libraries[26,29]. Stockwell lab observed that those two compounds were able to induce cell death in cells expressing oncogenic mutant HRAS and T oncoproteins the pattern of which appeared to be distinct from any other known cell death modality. In contrast to other forms of cell death, ferroptosis upon treatment with erastin or RSL3 resulted in rounded and detached cells with aberrant mitochondrial morphology[27]. In fact, it was revealed by electron microscopy that mitochondria lose structural integrity accompanied by increased mitochondrial membrane density and loss of cristae[30]. Contrary to apoptosis, nucleus morphology remained intact and no chromatin condensation was observed. The difference was further supported by studies showing that inhibitors of caspase, RIPK-1 or RIPK-3, known to prevent apoptosis and necrosis, have no inhibitory effects on ferroptosis[27]. However, a strong relation with cellular iron availability could be made. Indeed, ferroptosis is prevented by strong iron chelators. This concept associated to the protective effect of iron chelators and lipophilic antioxidants contributed to the definition of ferroptosis as a form of RCD operated by lipid peroxidation.

1.2.2.Molecular mechanism

In the following years, some mechanistic details of ferroptosis have been unveiled by using different classes of ferroptosis inducing agents (FINs). So far, the most upstream point of induction of ferroptosis is the inhibition of cystine (Cys-S-S-Cys) import via the cystine/glutamate transporter x_C^- [30]. System x_C^- is a heterodimeric protein complex in the plasma membrane composed of twelve transmembrane transporter protein SLC7A11 (xCT), linked to the single transmembrane regulatory protein SLC3A2 (4f2hc) by a disulfide bridge[31,32]. Although the flow is possible in both directions, in usual experimental conditions x_C^- antiporter allows the exchange of extracellular cystine with intracellular glutamate (Glu). Cystine that enters the cell is reduced by GSH or thioredoxin reductase 1 (TXNRD1) to cysteine (Cys) and used for GSH synthesis[33]. GSH is a tripeptide consisting of Glu, Cys and glycine (Gly) and is synthetized in two, adenosine triphosphate (ATP) dependent reactions. In the first reaction, the enzyme γ-glutamylcysteine ligase (GCL) catalyses the formation of γ-glutamylcysteine from Glu and Cys, the rate-limiting step of GSH synthesis. In the next step, glutathione synthetase (GS) adds Gly to γ-glutamylcysteine forming γ-glutamyl-cysteinyl-glycine.

GSH is used by oxidireductases and transferases as a nucleophilic substrate. In the specific case of GPx4, GSH is the nucleophilic substrate of the peroxidatic reaction of membrane lipid hydroperoxide reduction.

Notably, GPx4 is the only enzyme able to catalyse the reduction of complex hydroperoxides inserted in membranes into corresponding alcohols[28,34]. Thus, inhibition of the system x_C^- antiporter with small molecules such as erastin, imidazole ketone erastin (IKE) and sorafenib or direct inhibition of GSH synthesis with buthionine sulfoximine (BSO), will lead to lowering of cellular GSH concentration leading to insufficient GPx4 activity and finally membrane lipid peroxidation executing ferroptotic cell death[27,35,36].

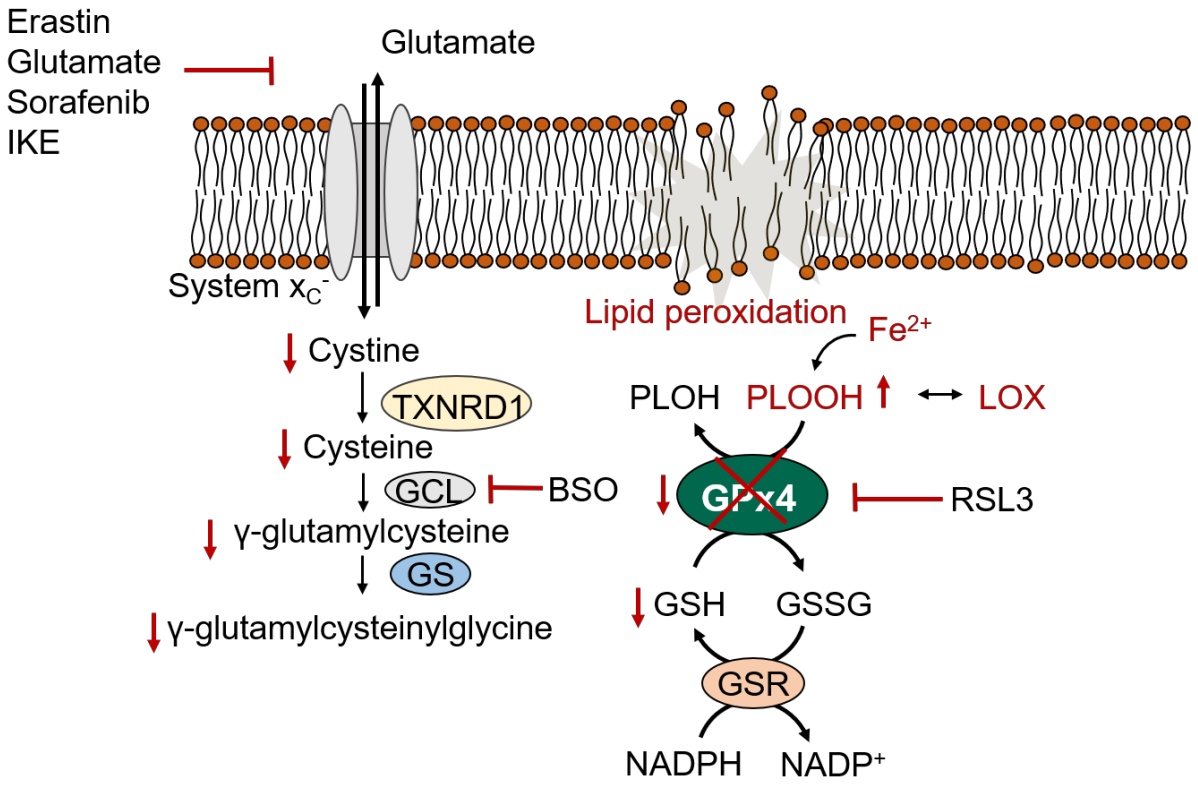

Figure 1. Mechanisms of ferroptosis induction
System x_C^- allowes the exchange of glutamate and cystine (Cys-S-S-Cys). When Cys-S-S-Cys enters the cell, it gets reduced into cysteine (Cys) by thioredoxin reductase (TXNRD1) or another molecule of GSH, and in such reduced form Cys is able to participate in GSH biosynthesis. When system $x_C^-$is inhibited by compounds such as erastin, glutamate, sorafenib or IKE, GSH synthesis is abrogated. BSO inhibits γ-glutamylcysteine ligase (GCL) and, likewise, leads to depletion of GSH, a substrate of GPx4. GPx4 uses two molecules of GSH that in turn gets oxidized (GSSG) but can be recycled by glutathione reductase (GSR) using reduced nicotinamide adenine dinucleotide phosphate (NADPH). Depletion of GSH, as well as direct inhibition of GPx4 by RSL3, leads to loss of function of GPx4 and accumulation of phospholipid hydroperoxides (PL-OOH) which in turn activate lipoxygenase (LOX) working on cell membrane phospholipids. These events lead to uncontrolled lipid peroxidation executing ferroptosis, when Fe^{2+} decomposes PL-OOH forming initiating radicals in the lipid phase.

Other ferroptosis inducing agents like (1*S*, 3*R*)-RSL3 (in text RSL3) are acting downstream of GSH depletion and are directly inhibiting the enzymatic activity of GPx4[24]. RSL3 because of its electrophilic chloroacetamide moiety is competent for a nucleophilic attack to amino acids such as Cys or Selenocysteine (Sec). Yang et al. provided evidence that RSL3 is capable for direct targeting of GPx4, which contains Sec in its catalytical active site resulting in inhibition of its peroxidase activity[37]. Accordingly, the observation that GPx4 is the target of RSL3 was further confirmed by knockdown and overexpression studies, demonstrating sensitization and strong resistance of cells respectively to RSL3 treatment. Thus, the inhibition of GPx4 emerges as a point of no return in the ferroptotic cascade.

1.2.3.Positive regulators of ferroptosis

1.2.3.1. Lipid peroxidation

Cellular membranes are composed of lipids. The unsaturation of different lipid classes is functionally extremely relevant in respect to biochemical and biophysical events and thereof polyunsaturated fatty acids are nutritionally indispensable. However, PUFAs are also particularly susceptible to oxidative degradation that can lead to loss of integrity of membranes, loss of cellular homeostasis and cell death[38]. As such, lipid peroxidation is seen as the critical event of ferroptosis and susceptibility of hydrogen abstraction from PUFA indispensable for the execution. In this respect it has been elegantly shown that cells pretreated with PUFAs where the heavy hydrogen isotope deuterium substitutes for hydrogen (D-PUFA) were resistant to lipid peroxidation and ferroptosis, due to increased energy of the carbon-deuterium bond over the carbon-hydrogen one[37].

Oxidative damage of lipids or lipid peroxidation is a complex series of reaction where lipids are degraded to a series of compounds all derived from hydroperoxides. In a comprehensive view, lipid peroxidation consists of three stages:

i) initiation, when the first radical is produced,
ii) propagation, where oxygen is added in a chain reaction and the number of radicals remains constant
iii) termination when the number of radicals decreases by radical-radical interaction

PL-OOH unavoidably and continuously produced during aerobic metabolism are the most relevant initiators of peroxidative chain reactions, when a lipid radical is formed in the membrane[39]. The initiating free radical is generated from PL-OOH by metals like iron (Fe^{2+}) breaking the O–O bond and forming the extremely reactive alkoxyl radical (PL-O$^{\bullet}$) in a Fenton-like reaction.

$$PL\text{-}OOH + Fe^{2+} \rightarrow PL\text{-}O^{\bullet} + Fe^{3+}\ H_2O$$

The alkoxyl radical generates the carbon centered radical $L^{\bullet}$

$$PL\text{-}O^{\bullet} + PL\text{-}H \rightarrow PL\text{-}OH + PL^{\bullet}$$

or, rearranges forming an epoxy group and a carbon centered radical in the fatty acid chain. Irrespective the presence of the epoxy group, the carbon centered radicals in the presence of oxygen forms a lipid hydroperoxyl radical ($PL\text{-}OO^{\bullet}$), which further by an H transfer generates another molecule of PL-OOH. When H is donated by a metylenic carbon of divinyl methane moiety of a fatty acid the formed carbon centered radical adds oxygen and propagates lipid peroxidation.

$$PL^{\bullet} + O_2 \leftrightarrow PL\text{-}OO^{\bullet}$$

$$PL\text{-}OO^{\bullet} + PL\text{-}H \rightarrow PL\text{-}OOH + PL^{\bullet}$$

During this propagation phase the number of radicals remains constant. The chain propagation is blocked with H donors, such as tocopherols (TOH) or coenzyme Q substituting for a PUFA. This reaction is defined as chain breaking since the antioxidant radical (e.g. tochopherol) is not capable to propagate the reaction.

$$PL\text{-}OO^{\bullet} + TOH \rightarrow PL\text{-}OOH + TO^{\bullet}$$

The chain breaking reaction although limiting propagation, favours the formation of PL-OOH since the oxygen addiction to a carbon centered radical is reversible. In this respect the reaction is also pro-peroxidant since from PL-OOH divalent metal ions initiate a new chain reaction. Thus, it is questionable whether the chain breaking reaction (i.e one electron reduction of $PL\text{-}OO^{\bullet}$) could be relevant for the inhibition of ferrous iron-dependent lipid peroxidation.

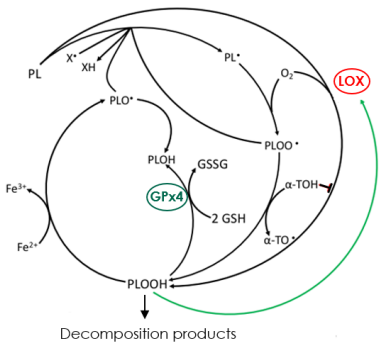

Figure 2. Scheme of lipid peroxidation controlled by GPx4

The phospholipid carbon centered radical ($PL^{\bullet}$) can be generated by i) an initiating radical ($X^{\bullet}$) ii) lipid hydroperoxyl radical ($PL\text{-}OO^{\bullet}$) in propagation reactions iii) alkoxyl radical ($PL\text{-}O^{\bullet}$) deriving from PL-OOH. Propagation reactions generates PL-OOH, which in turn gets reduced by GPx4 into alcohol (PL-OH). If not, PL-OOH in a Fenton type of a reaction with Fe^{2+} yields extremely reactive $PL\text{-}O^{\bullet}$. Furthermore, PL-OOH activate lipoxygenases (LOX) that produces more PL-OOH. PL-OOH generates decomposition products that can react with a variety of nucleophilic residues in protein residues and thereby impacting on their function. Image adapted from[40].

PL-OOH are rather unstable molecules breaking down during lipid peroxidation and forming a complex series of oxidized derivatives and fragmentation products such as reactive aldehyde species[40]. These species may induce lipid, protein and DNA modifications. Among these species the most studied is 4-hydroxynonenal (4-HNE). This electrophile modifies nucleophilic residues of essential signalling proteins and is detoxified by three aldo-keto reductase family 1, member C (AKR1C1-3). The formation of aldehydes has been suggested to be a critical mechanism for ferroptosis execution since overexpression of AKR1C1 is associated to resistance [41]. In line with the role of 4-HNE, it has been shown that an aniline based probe detected more than 400 endogenous proteins that undergo protein carbonylation during ferroptosis[42].

Besides slow oxidation linked to oxidative metabolism, PL-OOH can be generated also by lipoxygenases (LOX) that in turn are activated by PL-OOH. In mechanistic terms, the production of PL-OOH by LOX enzymes does not seem sufficient to induce *per se* ferroptotic cell death. It seems more reasonable, instead, that this enzymatic reaction by increasing the conversion of lipids to corresponding hydroperoxides deeply sensitize cells to ferroptosis, which anyway requires iron and missing GPx4 activity[43,44].This is in agreement with studies performed by Seiler et. al. where it was demonstrated that 12,15-LOX knock-out cells, are more resistant to cell death[45].
Likewise, increased expression of acyl-CoA synthetase long chain family member 4 (ACSL4) and lysophosphatidylcholine acyltransferase 3 (LPCAT3) that increase the amount of PUFA prone to lipid peroxidation will sensitize cells to ferroptotic cell death[46,47].

The free radical nature of lipid peroxidation supports the concept that free radical scavengers must prevent it. The notion that α-Tocopherol by scavenging PL-OO$^{\bullet}$ inhibits ferroptosis and substitute for GPx4 definitely is not convincing[48]. Scavenging of PL-OO$^{\bullet}$, indeed produces PL-OOH. Granted that α-Tocopherol in enormously supra-physiological concentration inhibit ferroptosis other mechanism must be taken into account: i) it reaches a concentration high enough to scavenge alkoxyl radical competing with a PUFA; ii) it prevents the initial formation of PLOOH; iii) it inhibits LOX acting on membrane phospholipids[49].

As a matter of fact, α-tocopherol is enormously less efficient to prevent ferroptosis than aryl-alkyl-amine molecules such as ferrostatin-1 (Fer-1) and liproxstatin-1 (Lip-1). These molecules known are extremely efficient ferroptosis inhibitors[49,50] and we recently show that this is due to the scavenging of alkoxyl radicals and the recycling of the radical form of the antioxidant[50].

1.2.3.2. Iron

The term of ferroptosis underscores the indispensable role of free-iron for initiation of lipid peroxidation that in turn leads to cell death[27]. The relevance of intracellular iron was proved by using chelators, or by adding iron to the growth medium in the form of iron bound to transferrin[51]. However, details of the role of iron in the mechanism of ferroptosis are not fully understood as well as it is not known whether modulation of iron availability could be a relevant determinant of ferroptotic death. The mechanism of iron is that previously described, where free Fe^{2+}, which in cells exist as "labile iron pool" (LIP), participates in Fenton type of reactions operating the cleavage of O-O bond of a phospholipid hydroperoxide (PL-OOH) forming the peroxidation initiating radical.

Iron is fundamental to life because it catalyzes redox transitions and interactions with oxygen which is necessary for cell growth and survival. Therefore, it is challenging to consider that iron is both, indispensable for life as well as to a form of regulated cell death.

Intracellular iron concentration and availability is carefully controlled by iron-regulatory proteins (IRP1 and IRP2), that can sense the cellular concentration of free iron and change the relative rate of uptake, storage, release and export[52]. Cellular iron uptake occurs via Fe^{3+} loaded transferrin (Tf) that binds to transferrin receptor (TfR) followed by endosomal uptake[53]. In the endosome, the acidification primes the release of Fe^{3+} from Tf followed by reduction to Fe^{2+} by six-transmembrane epithelial antigen of prostate 3 (STEAP3). Fe^{2+} is then transferred to the cytosol by divalent metal transporter 1 (DMT1) or ZIP8 and 14 (members of the solute carrier protein family 39) where it is associated to LIP[54]. LIP Fe^{2+} is either used in biosynthetic pathways or is sequestered by ferritin, an iron storage complex. To maintain iron cellular homeostasis, ferritin can undergo the process of autophagy, suggested to contribute to ferroptosis as it results in release of free iron[55].

Furthermore, the evidence that ferroptosis can be induced by an increase of Fe^{2+} generated upon increased expression of heme oxygenase-1 (HO-1) is in line with the notion of a pro-ferroptotic role of Nrf2 transcription factor in regulating HO-1 expression and thus iron concentration in the LIP[56,57].

1.2.4. Negative regulators of ferroptosis

1.2.4.1. PIP, PHGPx, GPx4

More than 50 years ago, Hochstein and Ernster described enzymatic reactions of iron dependent lipid peroxidation in microsomes[58]. In the following years, it was proved that lipid peroxidation is causing major oxidative damage to cellular structures and as such is involved in cellular pathological events[59]. Thus, McCay and colleagues gained a great deal of attention by demonstrating an existence of an inhibitor of lipid peroxidation present in rat liver extracts[60,61]. In

1973, they reported a GSH-dependent thermolabile protein able to control lipid peroxidation and speculated that the selenium dependent tetrameric glutathione peroxidase 1 (GPx1) already known for its peroxidase activity on small, soluble hydroperoxides could be somehow involved.

In 1982, Ursini and colleagues discovered the protein able to inhibit lipid peroxidation in liposomes and membranes[34]. Due to its function the enzyme was named Peroxidation-Inhibiting-Protein (PIP). PIP's reducing activity on phospholipid hydroperoxides was described by a uni-ter ping pong mechanism, similar to the mechanism already defined for GPx1[62]. However, PIP could also reduce phosphatidylcholine hydroperoxide (PC-OOH), cholesterol and cholesterol ester hydroperoxides inserted in membranes and this type of specificity was not mutual with any of the known peroxidases[63]. Thus, to accentuate the enzymatic role of PIP, in 1984 the enzyme was given a name 'Phospholipid Hydroperoxide Glutathione Peroxidase' (PHGPx)[28].

Today eight GPxs are known and PHGPx was systematically classified as glutathione peroxidase 4 i.e. GPx4[64].

1.2.4.1.1. GPx4 structure

GPx4 is a monomeric protein that at the tertiary protein structure level bears an extended thioredoxin fold[65]. This α/β motif can also be found in thioredoxins, glutaredoxins, glutathione S-transferases and the protein that catalyzes disulphide formation-Dsba[66]. Thus, the thioredoxin fold is common for five different protein families which, from a biological and functional point of view, do not share any specific function. However, all of them belong to the enzymatic class of oxidoreductases.

The thioredoxin fold is consisted of four stranded beta-sheets and three flanking alpha-helices yielding a two layers α/β/α sandwich with a β1α1β2α2β3β4α3 secondary structure pattern[66]. In GPx family members, the thioredoxin fold contains additional elements: two β-sheets at the N-terminus and one additional α-helix and β-sheet between β2 and α2. Furthermore, in tetrameric GPxs there is an extra aminoacid stretch positioned between α2 and β3, absent in monomeric GPx4.
The active site of GPx4 is the same as in other SecGPx, containing strictly conserved amino acids - Gln, Asn and Trp. The catalytic site of GPx4 lies in a flat area on the protein surface making it accessible to complex lipid hydroperoxides. In addition, analysis of human GPx4 structure shows that besides the positively charged area close to the peroxidatic Sec, there is another cationic area that is expected to contribute to the binding of exposed polar heads of phospholipids.

1.2.4.1.2. GPx4 kinetics and catalytic mechanism

Glutathione peroxidases are enzymes relying on either Sec or Cys catalysis[67]. In mammals, the first four (GPx1-4) and the sixth (GPx6) homologs contain Sec in catalyticaly active site, while in the other three enzymes (GPx5, GPx7 and GPx8) Cys substitutes for Sec.

GPx4 enzymatic catalysis follows the kinetic pattern of the first described SecGPx - GPx1, despite of the different substrate specificity[62]. Their catalytic mechanism is described as a ping-pong mechanism consisted of two events: oxidation of the reduced enzyme by a hydroperoxide, followed by a two-step reduction of the oxidized form by GSH[68,69]. In other words, the Sec selenol (E) in the active site is oxidized by R-OOH substrate which is being reduced into the corresponding alcohol followed by the reduction of the oxidized enzyme[68]. The reduction of the oxidized intermediate (F) take place in two successive steps: i) first, yielding the glutathionylated enzyme in the catalytic site (G), *i.e.* a selenodisulfide; ii) second, where selenodisulfide is reduced by a second GSH molecule forming GSSG and releasing the reduced catalytic selenium in the form of selenol (E) ready for the next cycle.

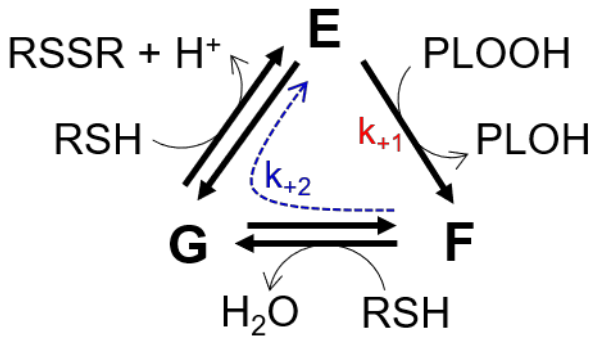

Figure 3. Scheme of GPx4 catalysis
The ground state enzyme (E) contains selenol in the active site and is oxidized by a hydroperoxide forming an intermediate (F), probably selenenic acid. In the next reaction, F is reduced yielding another intermediate (G) containing selenodisulfide in the active site. In the second reduction reaction, GSH releases the catalytic selenium in the form of E, i.e. selenol. k_{+1} and k_{+2} are rate constants for the net forward oxidative and reductive part of the catalytic cycle. Figure adapted from[69].

The catalysis of GPx does not fit with the Michaelis-Menten reaction kinetics. Instead, the reactive catalytic moiety suggests that the redox transitions occurring in the catalytic pocket are faster than the formation of typical enzyme-substrate complex[68]. Thus, SecGPx kinetics theoretically reaches infinite Vmax and Km values. The pertinent Dalziel equation that describes this kinetic pattern is:

$$[E0] / v0 = 1 / k'_{+1} \cdot [ROOH] + 1 / k'_{+2} \cdot [GSH]$$

where k'_{+1} and k'_{+2} are rate constants for the net forward oxidative and reductive part of the catalytic cycle. For SecGPxs, k'_{+1} rate constant for the oxidizing step is among the fastest enzymatic reactions ever measured. The reductive part is the rate-limiting step of the catalysis.

Recently, the catalytic cycle of GPx4 was described in atomic detail by density functional theory (DFT) method which allowed to obtain the energetic profile along the entire catalytic cycle, including intermediates and transition states[69]. The results showed that during the oxidative step of the catalytic cycle, a deprotonated intermediate of selenol is formed which is stepwise oxidized to selenenic acid. Absence of activation energy in this step comply with the elevated k_{+1} value measured by steady-state kinetics for the oxidizing step and provides evidence that the selenenic acid derivative of Sec really is the oxidized Se form in GPx. The energetic profile of CysGPx is similar to the one described for SecGPx, except for the formation of sulfenic acid instead of selenenic acid and comprehensive higher activation energies, which is in agreement with the lower efficiency of sulfur versus selenium catalysis.

During the reductive step of the catalysis, the DFT calculations confirmed that the enzyme forms the selenenylsulfide (or disulfide for CysGPx) intermediate which in the presence of a second molecule of thiol regenerates the ground state enzyme. The second reductive step having the highest activation energy is the rate-limiting reaction of the cycle. Furthermore, DFT calculations implied that the lack of reducing substrate leads to an oxidized intermediate 2 atomic mass units lighter that the reduced ground form. This intermediate contains selenium integrated as selenenylamide (Se-N) in a relaxed 5 or 8-membered ring generated by the interaction of selenenic acid with the downstream peptide nitrogen at the backbone of the enzyme. When the reducing substrate becomes available again, the thiolysis of the Se-N bond leads to the formation of Se-disulfide, which continues the catalytic cycle. In other words, the formation of selenylamide protects SeGPx from inactivation by over-oxidation. Notably, an analogous formation of sulfenylamide has been ruled out by quanto-mechanical calculation as it has been not analitycally detected. This further highligths the notion that the important advantage of selenolate- versus thiolate-based catalysis lies in its resistance to overoxidation.

Recently, Ingold et al. using a transgenic animal model confirmed the critical relevance of selenolate-based GPx4 catalysis in respect to thiolate-based catalysis[70]. It has been shown that Cys-GPx4 variant undergoes over-oxidation and inactivation differently from Sec-GPx4 which is resistant and that this resistance to oxidative inactivation is indispensable for controlling ferroptotic cell death. In this unique animal model, indeed, substitution of Cys for Sec produces severe alterations in embryogenesis incompatible with life and, only in a specific genetic background, a deadly neonatal neurodegeneration. At cellular level, the contemporary deletion of all 25 selenoproteins did not have

impact on cell survival as long as a minimal residual GPx4 activity is conserved in cells expressing the Cys-GPx4 variant. Thus, GPx4 is unique and first ranking in the account for the indispensable nature of selenium[70].

1.2.4.2. GSH

GSH, the reducing substrate of GPx4, is indispensable to life. Indeed, mice lacking γ-glutamylcysteine ligase (GCL) die at the same developmental stage as GPx4 knock-out mice[71].

The relevance of GSH in ferroptosis emerged from studies on cancer cells using small molecule erastin, which irreversibly inhibits the cellular import of cystine through x_C^-, necessary to sustain GSH levels[27]. Being x_C^- a bidirectional antiporter, the net flow of metabolites is controlled by the concentration of glutamate and Cys[72].Thus, high concentrations of extra cellular glutamate will block cystine import and cause cell death by GSH deprivation. This is likely relevant for neuronal cell death induced by high concentrations of glutamate described almost 20 years ago and named oxytosis[73]. Oxytosis encompasses GSH depletion, activation of LOX and increased lipid peroxidation, common features of ferroptosis. Although a peculiar distinctive and additive feature of oxytosis in the increase of intracellular calcium, oxytosis and ferroptosis are probably representing the same form of RCD[74].

In addition to system x_C^-, several cells use other amino acid transporters for cysteine uptake or, alternatively, generate Cys from methionine in the transulfuration pathway[75]. Transulfuration pathway converts methionine to homocysteine which further gets converted to cystathionine and finally Cys. This pathway, activated by cystenyl-tRNA synthetase (CARS) knock down, has recently been shown to have a role in the protection against ferroptosis induced by system x_C^- inhibitors[76,77]. Furthermore, cystathionine has recently emerged as a novel substrate of the system x_C^- able to regulate extracellular glutamate concentration and cystine availability in the brain[78]. Thus, exchange of cystathionine through system x_C^- is probably increasing intracellular GSH concentration thereby contributing to the maintenance of the oxidative homeostasis of the cell.

Moreover, GSH biosynthesis is under the control of Nuclear factor erythroid 2-related factor 2 (Nrf2) transcription factor, the key regulator of the cellular response against different challenges, including oxidative stress[79]. Electrophiles created during oxidative stress will react with nucleophilic Cys residues of Kelch like-ECH-associated protein 1 (Keap1) and disrupt the constant ubiquitination of Nrf2[80]. The accumulated Nrf2 will transfer to the nucleus and upregulate the expression of GCL and GSH synthesis. Likewise, Nrf2 upregulates the expression of system x_C^- and create an efficient reducing cystine/cysteine cycle thereby protecting from cell death[81].

To prevent cell death, some cells like astrocytes, can secrete GSH into extracellular space by multi-drug resistance proteins (MRP) and provide GSH for other cells like neurons[82]. In that case, secreted

GSH is cleaved by γ-glutamyltranspeptidase (GGT) releasing Glu and cystenylglycine[83]. GGT transfers Glu to other amino acids and the cystenylglycine dipeptide gets hydrolysed by a dipeptidase (DP) releasing Cys and Gly. Free Cys and Gly, as well as γ -glutamyl amino acids, can then be taken up by various transporters from neurons and used for GSH synthesis. Cys that in return gets oxidized into cystine can be re-used by astrocytes by system x_C^-.

Besides GSH, MRPs can export oxidized glutathione (GSSG), as well as GSH adducts generated by glutathione transferases (GST). In that manner GSTs detoxify a variety of aldehydes and electrophiles created during cell metabolism. In fact, the induction of MRP1 has been demonstrated to be neuroprotective[84]. Nevertheless, in some studies the major reported biological effect of MRP is the depletion of intracellular GSH and this intrinsically represents a risk of poorly controlled oxidations and related toxicity and death[85,86].

Taking all this set of information as a whole, we must recognize that the relevance of the physiological regulation of MRP must be rated as still poorly clarified, while there is no doubt that GSH concentration is of pivotal relevance in controlling ferroptosis.

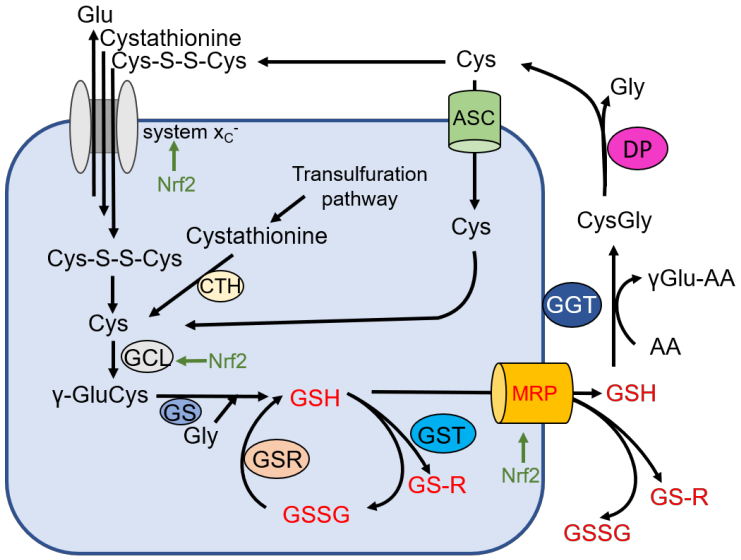

Figure 4. Overview of GSH metabolism

System x_C^- allows the entrance of Cys-S-S-Cys, which in its reduced form Cys participates for GSH synthesis. GSH synthesis consists of two steps: 1) enzyme γ-glutamylcysteine ligase (GCL) catalyses the formation of γ-glutamylcysteine from Gln and Cys; 2) glutathione synthetase (GS) adds Gly to γ-glutamylcysteine forming GSH. Furthermore, Cys that participates in GSH synthesis can be re-synthesized by transulfuration pathway. Nrf2 transcription factor (indicated by green arrows) induces the transcription of system x_C^-, GCL but also multi drug resistance proteins (MRP) that export GSH, oxidized GSH (GSSG) and GSH conjugates (GS-R). In extracellular environment, γ-glutamate transpeptidase (GGT) transfers the γ-glutamate to other amino acids, forming CysGly. Peptide bonds between Cys and Gly are hydrolyzed by a dipeptidase (DP) forming Cys and Gly. Cys can be taken up by system alanine-serine-cysteine (ASC), or, if oxidized, by system x_C^-. Furthermore, cysteine availability in the cell can be regulated by cystathionine.

1.2.5. Relevance of ferroptosis in different diseases - possible pharmacological targeting

After ferroptosis has been described in 2012, accumulating evidence suggested that ferroptosis could be the cell death mechanism occurring in neurodegenerative disorders such as Huntington's, Alzheimer's Parkinson's disease and amyotrophic lateral sclerosis, and that it could be the also the driver of neuropsychiatric conditions such as schizophrenia, bipolar disorder and depression[87–92]. This is in agreement with studies that revealed that in a mouse model of Alzheimer's disease expression of GPx4 was downregulated and accompanied with an increase of lipid peroxidation by-products[93]. Moreover, studies using heterozygous GPx4 knock-out mice showed increased levels of lipid peroxidation products in the brain, as well as increased numbers of amyloid plaques, a hallmark of Alzheimer's disease[94]. Another group reported that conditional knock-out of GPx4 in the brain induced neurodegeneration[95]. In fact, neurons seem to be susceptible to lipid peroxidation and ferroptotic cell death as revealed by many studies related to neurological disorders.

Besides, many other studies using conditional GPx4 knock-out models have implicated that GPx4 has a crucial role in T cell immunity, reticulocyte maturation, hair follicle morphogenesis, vascular homeostasis and is essential for protection of retinal degradation and organ failure induced by ischemia reperfusion [22,96–100]. Furthermore, ferroptosis has been shown to have a role in bacterial infections like sepsis or tuberculosis, as well as in viral diseases[101–103]. All these studies indirectly point out that ferroptotic mechanisms could play a role in chronic disease or degeneration of the respective tissue.

In addition, the regulated character of ferroptosis is an appealing therapeutic approach for anticancer strategy. It is known that tumours rely on iron rich microenvironment necessary to support proliferation[104]. Thus, controlling iron levels could be a potential approach for ferroptosis inducing anticancer therapy[105]. Furthermore, Wu et al demonstrated that mesenchymal or metastatic cells cancer cells are very sensitive to ferroptosis[106]. Genetic inactivation of tumor suppressor neurofibromin 2 (NF2) rendered cancer cells more prone to ferroptosis in mouse model of malignant mesothelioma. Additional recent evidences have shown that p53 tumor suppressor has a dual role in ferroptosis. Jiang et al. suggested that p53 impedes the expression of SLC7A11, a subunit of system x_C^- antiporter, thereby inhibiting cystine uptake and inducing increased sensitivity to ferroptosis[107]. On the other hand, p53 upregulation inhibits ferroptosis in certain cell types by increasing the transcription of antioxidant genes or via effects on p21 associated with slower depletion of intracellular glutathione and reduced lipid peroxidation[108].

To sum up, understanding the mechanism of ferroptotic cell death is expected to help in development of novel therapies that will halt cell death in degenerative processes or activate it in cancer cells.

2. AIM OF STUDY

Differently from other forms of RCD, for ferroptosis a unique pathway enrolling specific protein signalling cascade has not been described and seemingly does not exist. At the present level of knowledge, ferroptosis is seen as the outcome of an insufficient activity of GPx4, eventually leading to lipid peroxidation.

In typical ferroptotic model systems GPx4 is either missing or its activity is depressed by lowering the concentration of its reducing substrate. GPx4 is also inhibited by a series of electrophiles, the prototype of which is the drug candidate RSL3. Besides low or absent GPx4 activity, only two major indispensable constraints for the activation of ferroptosis have been clearly identified: i) content of polyunsaturated fatty acids in membrane phospholipids; and ii) availability of Fe^{2+}in LIP.

This study was aimed to the identification of other more subtle physiological constraints to be fulfilled for the execution of ferroptosis, conceived as a relevant physiological event intrinsically linked to aerobic metabolism.

We were particularly interested to unravel in the site of production of and the mechanism of reactions leading to the indispensable formation of traces amounts of PL-OOH from which iron initiates lipid peroxidation when GPx4 is insufficient. In the working hypothesis we identified for this event the metabolism of oxygen in mitochondria.

We also aimed to achieve evidence about the possible physiological relevance of inhibition of GPx4 by electrophiles. In our working hypothesis, indeed, RSL3 could be just a pharmacological mimic of a still unknown species competent for operating this form of RCD. This hypothesis was stimulated by the observation that purified GPx4 is not inhibited at all by RSL3, suggesting the existence of a more complex physiological process for the control of GPx4 activity and hereto ferroptosis.

3. RESULTS AND DISCUSSION

3.1. AIM 1 - Role of mitochondrial respiration in ferroptosis

3.1.1. Cell density regulates sensitivity to ferroptosis

Initially, we confirmed in HT1080 cells the previously reported observation that cell density impacts on sensitivity to ferroptosis. Indeed, also our cells plated at low density were sensitive to ferroptosis induced by erastin, while cells plated at high density were resistant (Fig. 5A). Furthermore, in order to link cell density to free radical oxidations, assumed to be associated to lipid peroxidation taking place in the lipid phase, we used the oxidation sensitive fluorescent dye BODIPY C11. Consistent with the basic notion, we observed an inverse correlation of cell density with free radical oxidations in membranes of cells (Fig. 5B). Cells plated at high density didn't show any increase of the signal upon erastin treatment. Thus, we concluded that cells at high density must have changed their metabolism in a way hampering lipid peroxidation and ferroptosis.

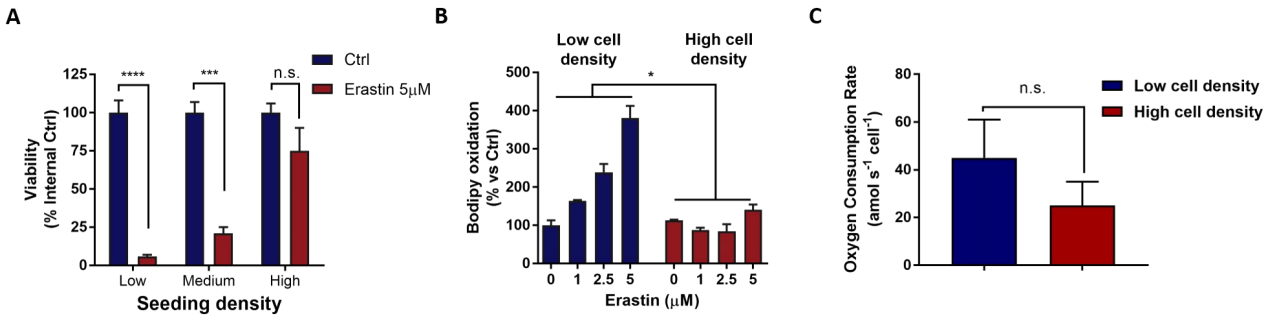

Figure 5. Cell density impacts on sensitivity to ferroptosis

(A) High-density seeded cells are resistant to erastin induced ferroptosis. Cells were seeded at low (3000 cells/well), medium (25 000 cells/well) and high (50 000 cells/well) density in a 96 well plate and treated with 5 μM erastin for 24h. Resazurin reduction rate was evaluated as AFU/min and expressed as % of control.

(B) Cells plated at high density doesn't show increased BODIPY oxidation followed by flow-cytometry analysis after 9h of erastin treatment.

(C) Oxygen Consumption Rate (OCR) is dependent on cell density. OCR was measured using MitoXpress.

All data are presented as mean ± SD of n=3 different experiments. (*p < 0.05, **p < 0.01, ***p < 0.001, ****p < 0.0001, n.s.=not significant; one-way ANOVA).

Owing the critical role of oxygen in peroxidation, the first, obvious, candidate to account for relationship between cell density and ferroptosis was the oxygen consumption rate (OCR).

Our measurements failed to reveal a significant linear correlation between OCR and cell density, although the difference between maximal and minimal cell density was still supporting the notion that cell density negatively impacts on OCR (Fig. 5C). Indirectly the notion that oxygen metabolism could influence sensitivity to ferroptosis was still not ruled out and worth of further investigation.

3.1.2. Electron flow through the respiratory chain does not affect sensitivity to erastin induced ferroptosis

According to the basic axiom of ferroptosis, production of traces of PL-OOH is a positive permitting constraint. The granted mechanism is a free radical oxidation of a PUFA in a phospholipid, followed by oxygen addition and hydrogen transfer (see introduction). The most likely radical producing a free radical oxidation in the membranes is the perhydroxyl radical ($HO_2^{\bullet}$), the protonated form of $O_2^{\bullet-}$[109].

It is known from decades of studies that during electron transfer from substrates to oxygen, some electrons may leak from their transporters and reduce O_2 to superoxide anion $O_2^{\bullet-}$, the precursor of the so called "reactive oxygen species" (ROS)[110]. In the most acknowledged view, $O_2^{\bullet-}$ is produced mainly from complex I and complex III of the respiratory chain. Thus, to examine whether this is also a critical constraint of ferroptosis we planned experiments aiming to disclose the possible relationship between electron flow and sensitivity to ferroptosis primed by erastin.

In these experiments we used inhibitors of respiratory chain facilitating electron leaks, and an uncoupler of oxidative phosphorylation. We considered both, the intrinsic toxicity and the effect on ferroptosis primed by erastin, i.e, GSH depletion. The specific occurrence of ferroptosis was evaluated by the protective effect of Fer-1.

Rotenone is a well-known inducer of $O_2^{\bullet-}$production that binds the CoQ -binding site of complex I. It decreases the cellular respiration by limiting the electron transport and thereby induces electron leaks and the production of $O_2^{\bullet-}$. We used rotenone at concentrations validated as sufficient to inhibit the respiratory chain activity. As shown in Fig. 6A, 0.5 µM rotenone deeply decreases the OCR but is ineffective on ferroptosis induced by erastin (Fig. 6B), although producing an unspecific toxic effect impacting on proliferation, which is insensitive to Fer-1, the benchmark of specificity of ferroptotic death (Fig. 6C).

Complex III inhibitor, antimycin, was examined following the same approach. Antimycin inhibited OCR (Fig. 6D) but this didn't impact on sensitivity to ferroptosis (Fig. 6E). Moreover, Fer-1 doesn't inhibit the effect of antimycin on cell viability (Fig. 6F).

To further evaluate the hypothesis about the possible role of electron leaking from the respiratory chain in ferroptosis, we treated cells with Carbonyl cyanide-4-(trifluoromethoxy) phenylhydrazone (FCCP), an uncoupling agent that increases the OCR and thus the rate of the transfer of electrons to O_2. We observed that 0.3 µM FCCP although sufficient to increase OCR by 30% did not have any effect on ferroptosis (Fig. 6G and H).

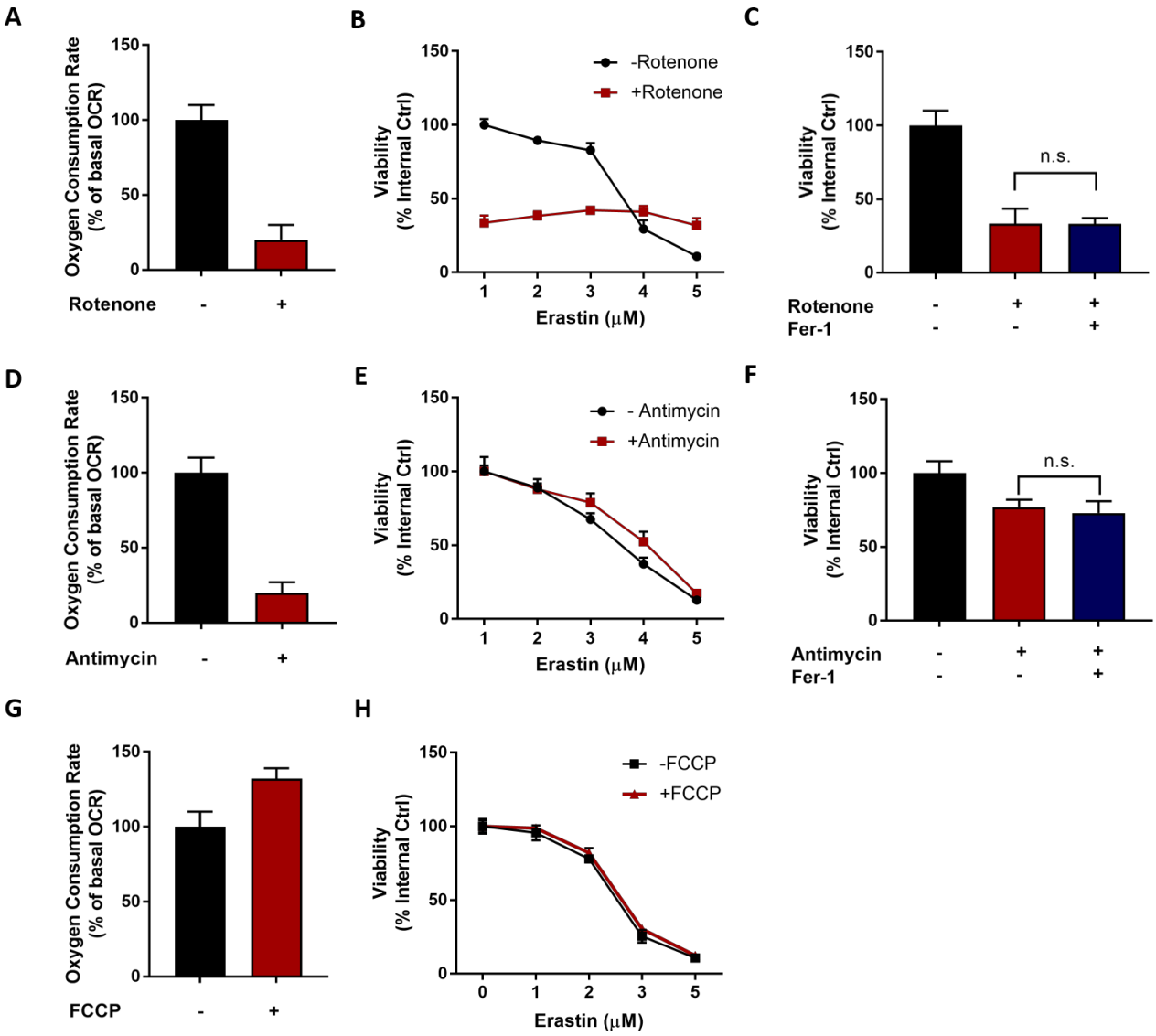

Figure 6. Electron transport chain is not relevant for ferroptosis

(A) 0.5 μM rotenone is sufficient to decrease the OCR.
(B) Co-treatment with 0.5 μM rotenone doesn't affect ferroptosis induced by various erastin concentrations.
(C) Fer-1 doesn't protect from rotenone induced cell death
(D) 1 μM of antimycin effectively inhibits the OCR
(E) Inhibition of complex III doesn't affect ferroptosis response in cells treated with erastin
(F) Fer-1 cannot prevent the antimycin effect on cell viability
(G) 0.3 μM FCCP induces the maximal respiration rate in HT1080 cells
(H) Uncoupling of the respiratory chain doesn't sensitize cells to ferroptosis.
(A, D, G) The mitochondrial OCR was measured using XF Extracellular Flux Analyzer (Seahorse analyzer). OCR was expressed as % of the basal respiration rate.(B, C, E, F, H) Cell viability was assessed by measuring the resazurin reduction rate evaluated as AFU/min and expressed as % of the corresponding control. All data are presented as mean ± SD of n=3 different experiments (n.s.=not significant, one-way ANOVA).

In summary, from this set of evidence we reached the conclusion that the electron flow in the respiratory chain of mitochondria is not a relevant constraint for ferroptosis induction in HT1080 cells.

3.1.3. Role of Glutamine and α-Keto Acids for the induction of ferroptosis

In agreement with the notion that mitochondrial activity could play a role in ferroptosis it has been shown that glutaminolysis is necessary for ferroptosis induced by GSH depletion[51]. We confirmed this intriguing evidence in our cellular model (Fig.7A). Glutamine (Gln) by glutaminolysis provides substrates of dehydrogenases participating to the Krebs cycle (Fig 7B). To test the relevance of this pathway downstream of glutaminolysis we substituted α -ketoglutarate (α-KG) for Gln and we reproduced the effect on ferroptosis (Fig. 7C). Intrigued by this stimulating evidence we speculated about a role of Krebs cycle in the necessary support of ferroptosis induced by erastin. The non-ambiguous experimental evidence was that malonate (supplied as dimethyl ester) blocking the Krebs cycle had no effect on ferroptosis (Fig. 7D). This ruled out the role of Krebs cycle, at least when fed with endogenous substrates.

The conclusion was that it is the activity of α-KG dehydrogenase having this role when interacting with relatively high substrate concentration. Apparently, when only endogenous substrates fed the Krebs cycle the formation of the activity of the dehydrogenase is not sufficient to fulfil the constraint for the permission of ferroptosis primed by GSH depletion, i.e. the formation of the oxidant generating the required traces of PL-OOH.

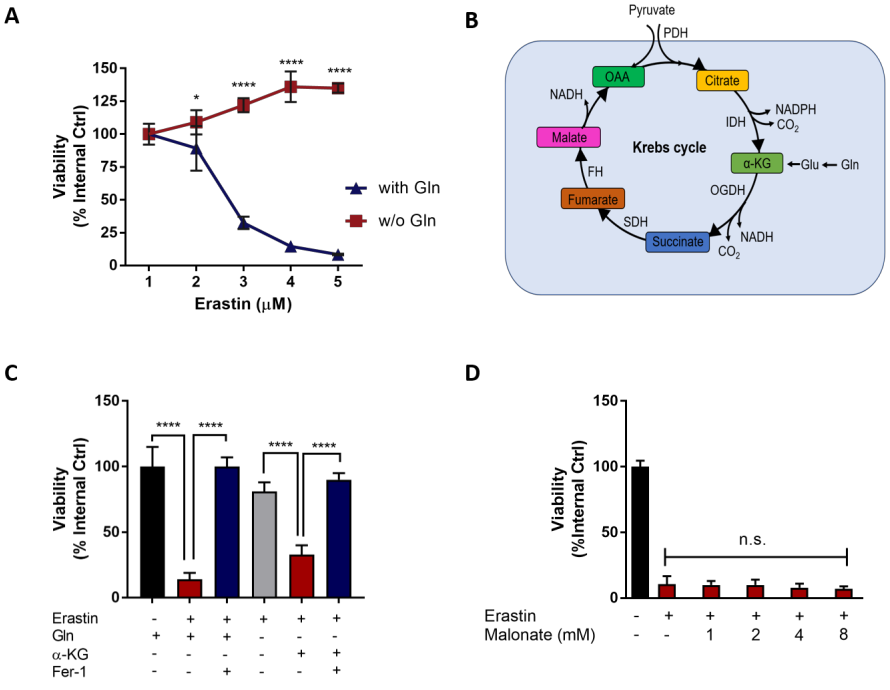

Figure 7. α-KG can replace Gln for induction of ferroptosis by erastin
(A) Gln is necessary for ferroptosis induction. Cells were treated with 5 μM erastin for 24h in presence or absence of 4 mM Gln and tested for cell viability.
(B) Basic scheme indicating the relation between Gln and Krebs cycle

(C) α-KG can replace Gln in supporting ferroptosis induction. Cell viability assay was assessed by resazurin sodium salt reduction of cells cultured in presence or absence of 4mM Gln. Where indicated, 8mM α-KG was used instead of Gln. Cells were treated with 5 μM erastin for 24h.
(D) Various concentrations of malonate have no effect on erastin induced cell death. All quantitative data are presented as mean ± SD of n=3 experiments (*p < 0.05, **p < 0.01, ***p < 0.001, ****p < 0.0001, n.s.=not significant; one-way ANOVA).

α-KG dehydrogenase complex (OGDC) is an enzyme formed of multiple copies of three components: oxoglutarate dehydrogenase (E1), dihydrolipoyl succinyltransferase (E2) and dihydrolipoamide dehydrogenase (E3)[111]. The OGDC has the same global structure and uses the same coenzymes as pyruvate dehydrogenase complex (PDC) and branched-chain keto-acid dehydrogenase complex (BCKDC). Therefore, we questioned whether HT1080 cells deprived of Gln could gain back their sensitivity to ferroptosis by supplementing the medium with specific α-keto acid dehydrogenase substrate. In fact, we observed that also pyruvate efficiently recapitulate the role of Gln in ferroptosis (Fig. 8A).

Last we tested α-ketobutyrate (α-KB), which is converted to propionyl-CoA by BCKDC. Consistently with other results, α-KB restored erastin induced cell death in cells deprived of Gln (Fig. 8B).

To better validate the interpretation of the results we tested if these substrates impact on GSH depletion brought by erastin. In samples containing Gln, 9h of erastin treatment depleted GSH by about 80% (Fig. 8C). We also noticed that samples without Gln and supplemented with pyruvate or α-KB, had already a decreased GSH content probably due to the lower availability of glutamic acid for GSH synthesis. Consistently, control samples treated with α-KG had a basal increased GSH concentration as a result of transamination reactions that regenerate glutamate. However, in all these conditions erastin treatment was able to decrease GSH levels with the same efficiency.

To test if α-KB, α-KG and pyruvate can substitute Gln for the production of oxidant radicals in membranes, we applied BODIPY C11 fluorescent probe. Indeed, an increased oxidation signal was observed using α-keto acids in respect to control cells without Gln (Fig. 8D).

This result corroborates the notion that OGDC, PDC and BCKDC are competent for the formation of oxidant radical species in the membranes necessary for activation of ferroptosis primed by GSH depletion.

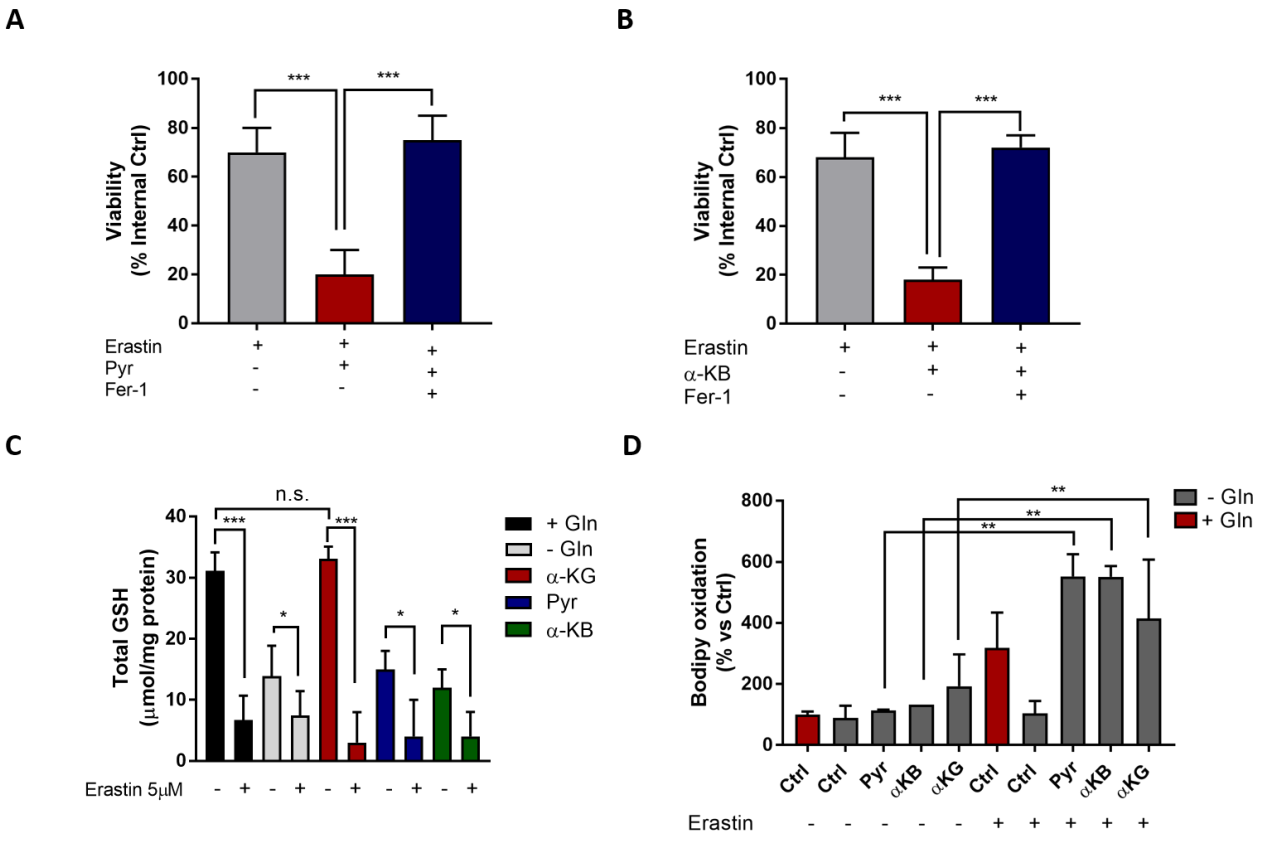

Figure 8. α-keto acids and induction of ferroptosis by erastin
(A) Pyr (10 mM) and (B) α-KB (10 mM) can replace Gln for the induction of ferroptosis. Cell viability was assessed using resazurin sodium salt reduction after treatment with 5 µM erastin for 24h.
(C) Total GSH measurement. Total GSH was assessed after 9h of treatment with 5 µM erastin.
(D) Increase of BODIPY C11 oxidation after 9h of 5 µM erastin treatment using cells without Gln (grey bars) and with Gln (red bars) and where indicated supplemented with 10 mM Pyr, 10 mM α-KB or 8 mM α-KG. All quantitative data are presented as mean ± SD of n=3 experiments (*p < 0.05, **p < 0.01, ***p < 0.001, n.s.=not significant; one-way ANOVA).

Although α-keto acid dehydrogenase complexes have a different keto acid specificity they catalyze the same sequence of reactions thereby generating CO_2, corresponding acyl-CoAs and NADH (Fig. 9)[112]. The first reaction of decarboxylation of the keto-acid is performed by a specific keto-acid E1 subunit using the cofactor thiamine pyrophosphate (TPP). The second reaction is operated by the E2 dihydrolipoamide acyltransferase that transfers the formed acyl group to CoA. The third reaction catalysed by E3 dihydrolipoamide dehydrogenase operates the oxidation of dihydrolipoamide bound to E2 and requires FAD^+ and NAD^+ as final electron acceptor. E3 is identical for each complex, while E1 and E2 are different proteins using the same cofactors to perform the individual reactions.

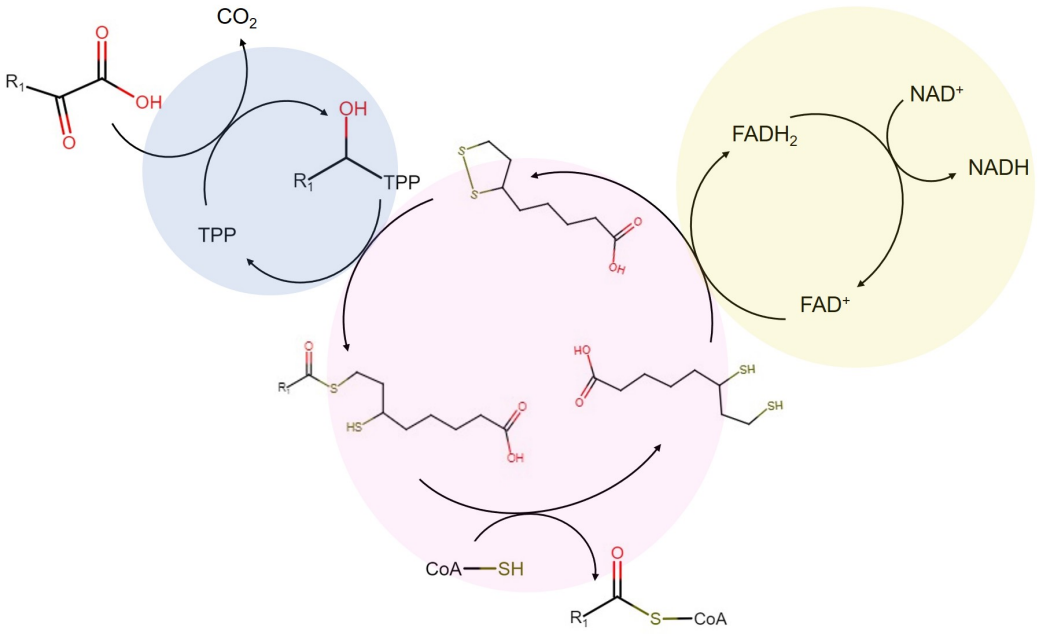

Figure 9. Reaction mechanism of α-keto dehydrogenases

α-Ketoacid dehydrogenase complexes consist of three subunits: keto acid dehydrogenase E1 (blue circle), ketoacid transacylase E2 (pink circle) and dihydrolipoamide dehydrogenase E3 (yellow circle). These complexes catalyse the reactions of decarboxylating the α-keto acid substrate to produce CO_2, acyl CoA and NADH. The reaction performed by E1 is the thymine pyrophosphate (TPP) dependent decarboxylation of the α-ketoacid yielding an TPP-intermediate. This reaction is followed by the transfer of reactive intermediate to a lipoyl moiety (LA-S_2) on the E2 subunit creating an acylated dithiol group. The E2 then transfers the acyl intermediate to CoA forming an acyl-CoA and dihydrolipoamide (LA-$(SH)_2$). FAD on the E3 subunit readily oxidizes the lipoyl group on the E2 subunit and generates NADH through coupled reactions of $FADH_2$ and NAD^+.

The complex binding lipoic acid has been shown to be competent for the formation of species of partial oxygen reduction transferring electrons from dihydrolipoyl residues on E2. Under limited NAD^+ and in the presence of reduced substrate, 1*e*- reduction of O_2 results in the formation of superoxide anion.

Having all of that in mind, we questioned whether silencing of the E3 subunit of the ketoacid dehydrogenases complexes would sensitize cells to ferroptotic cell death.

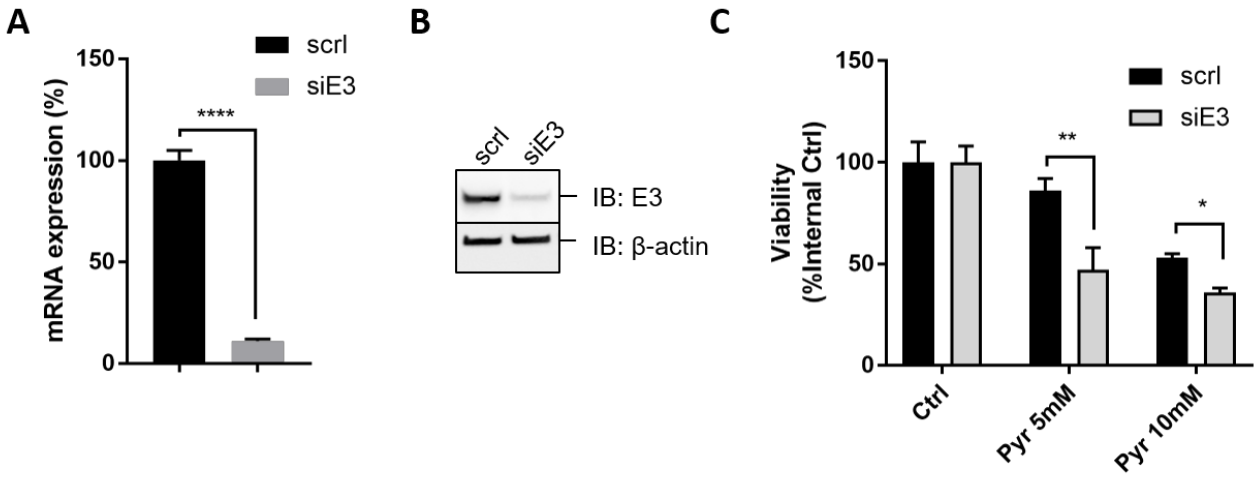

Figure 10. Silencing of E3 sensitizes cells to ferroptosis
(A) Gene expression analysis of scrambled (scrl) and silenced (siE3) cells.
(B) Western Blot analysis of scrambled (scrl) and silenced cells (siE3).
(C) Cell viability assay of scrl and siE3 cells treated with erastin (5 μM). Medium without Gln was used for control cells (Ctrl) and where indicated supplemented with Pyruvate.
Data are representing the mean of three independent experiments (*p < 0.05, **p < 0.01, ****p < 0.0001, n.s.=not significant; one-way ANOVA).

Obtained data clearly show that in E3 silenced cells (Fig. 10A and B) pyruvate sensitize cells to erastin induced ferroptosis (Fig. 10C).

Mitochondrial respiration is considered a main source of radical species production within the matrix of mitochondria. In our working hypothesis these radicals are competent for the formation of PL-OOH, which, if not immediately reduced, are decomposed by iron thus initiating series of lipid peroxidation events, eventually leading to ferroptosis.

Complex I and complex III site of the mitochondrial respiratory chain are described as one of the main sites of $O_2^{\bullet-}$ production associated with other types of regulated cell death[113]. Despite this, in this study we clearly demonstrate that $O_2^{\bullet-}$ production from these sources doesn't have a role in promoting ferroptotic cell death. Furthermore, also uncoupling or respiratory chain does not affect the death pathway operated by iron.

Altogether our data support the notion that the modulation of electron transport chain known to produce superoxide is not relevant for ferroptosis induction.

Our evidence that mitochondria are necessary for the execution of ferroptosis are in an apparent contrast with the notion proposed by Dixon et al that cells depleted of mitochondrial function are still sensitive to ferroptosis[27]. However, we have to point out that in these cells (ρ^0 cells) it is just the respiratory chain that is missing. We argue that, ρ^0 cells develop pyruvate auxotrophy to compensate

for the loss of mitochondrial respiration and to support metabolic needs for proliferation[114,115]. Nothing against, therefore, that pyruvate could continue to be oxidatively decarboxylated by pyruvate dehydrogenase and thus remains competent for the generation of traces of PL-OOH required for activation of ferroptosis in the presence of erastin. In summary, our data do not conflict with the evidence produced by Dixon. We both agree that respiratory chain has a minimal role, if any.

The notion that α-keto acids can recapitulate the effect of Gln in ferroptosis could be interpreted in respect the mechanism of formation of superoxide anion is produced during re-oxidation of dihydrolipoate bound to E2 in alternative to reduction of NAD^+.

Seemingly a competition exists between FAD and O_2 for accepting electrons. Granted that the vast majority of electrons are transferred to NAD^+ via FAD, it not unrealistic assuming that traces can escape the canonical pathway reducing O_2, as experimentally evidenced. It is also worth of consideration the notion that this event is more evident in the absence of E3.

Taken together, the formation of superoxide anion during re-oxidation of dihydrolipoate emerges as particularly relevant in respect the need of formation of the traces of PL-OOH from which lipid peroxidation can be initiated only when GPx4 is missing.

3.2. AIM 2. - Mechanism of inactivation of purified GPx4 by RSL3 as a nucleophile prototype

A large body of evidence converge to the notion that ferroptosis is activated when, provided the fulfilment of different constraints, GPx4 is inactivated.

A list has been compiled of compounds suggested inhibiting GPx4, of which the prototype is the drug candidate RSL3 (Table 1). This compound, indeed, has been the species that contributed to the identification of ferroptosis as a new form of regulated cell death. Notably, studies on inhibition of GPx4 have been carried out on cells and did not provide neither kinetic nor mechanistic insights about the enzymatic reaction.

(1*S*,3*R*) RSL3[24]	covalent inhibitor of GPx4 inducing loss of enzymatic activity
ML162, DPI compounds 7,10, 12,13, 17, 18,19[37,116]	covalent inhibitors of GPx4
FIN56[117]	induces decrease in GPx4 protein expression
FINO2[118]	induces loss of GPx4 activity

Table 1. Compounds modulating GPx4 activity or protein expression

Aiming to address this issue we resorted to fill the gap between cell biology and enzymology taking advantage of the availability of purified GPx4 in our laboratory. Results presented in this part of the thesis have been published in a FEBS Letters publication[119].

For inhibition experiments we used HEK293T cells as they have a high endogenous GPx4 specific activity which allows more accurate measurement of inhibition compared to HT1080 cells. Indeed, we confirmed that RSL3 inhibits GPx4 specific activity in our cell model (Fig. 11).

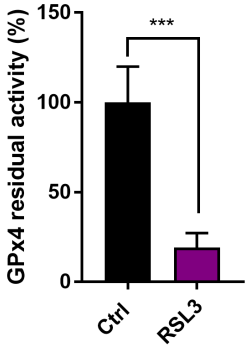

Figure 11. RSL3 decreases GPx4 specific activity in HEK293T cells
Gpx4 specific activity was measured on 200 µg of the cytosol proteins after 2h of treatment with 0.75 µM RSL3. Data are presented as mean ± SD of n=3 experiments (***p < 0.001, two-tailed, unpaired t-test with Welch's correction).

Surprisingly, however, we did not observe any inactivation of GPx4 by RSL3 on the purified enzyme. Actually, purified GPx4 was inhibited by RSL3 only by extending the time of incubation with the compound up to 24 hours, and similar results were obtained with the diastereomer 1*R*,3*R* RSL3. Therefore, the inactivation was considered as nonspecific and biologically not relevant.

On the other hand, the inactivation was observed in the presence of freshly prepared HEK293T cell cytosol. We also noticed that this inactivation permitting activity of the cytosol diminished over time and that a presence of a reducing agent in the cell cytosol, 2.5 mM GSH or TCEP, could prevent this progressive loss of efficiency.

The inactivation of GPx4 by RSL3 depends on the amount of cytosolic proteins (Fig. 12A), concentration of RSL3 (Fig. 12B) and time of incubation (Fig. 12C).

The standardized experimental conditions for quantifying the GPx4 permitting activity in the presence of RSL3 were as follows: 0.5 mg/mL of cytosol proteins, 100 µM RSL3 and 20 minutes incubation. Under these conditions GPx4 is usually inactivated at 60-70% (Fig. 12A-C).

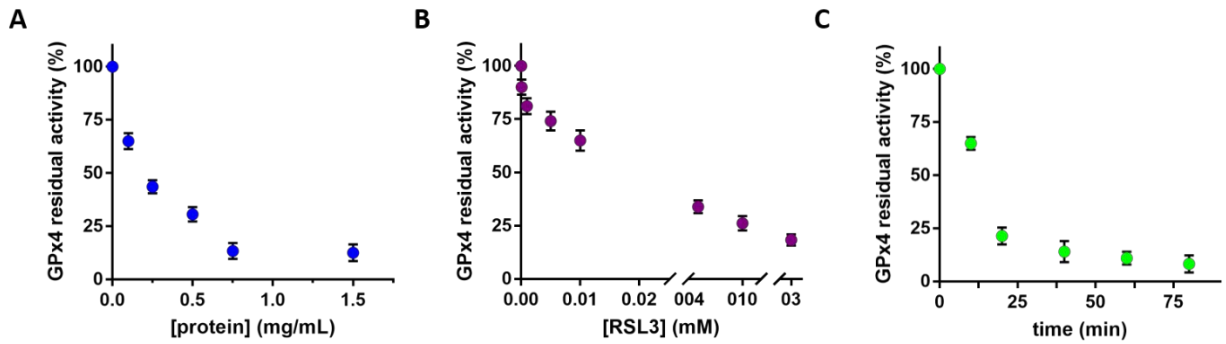

Figure 12. Determinants of GPx4 inactivation by RSL3
Effect of concentration of cytosolic proteins (A); incubation time (B); RSL3 concentrations on inactivation-permitting activity (C). All inactivation tests contained 50 nM of GPx4. The other determinants were varied one at a time, keeping the other two fixed: protein concentration 0.05 mg/mL; RSL3 concentration 100 µM, time 20 minutes. Results are expressed as the percentage of residual enzyme activity. Data represent the mean ± SD of n=3 experiments.

Since a reducing agent was necessary to preserve the inactivation-permitting activity in the cell cytosol, we hypothesized a redox transition in the protein impacting on activity. We tested this using diamide, a thiol oxidizing agent, specifically producing disulphides among thiols at compatible distance. In fact, diamide abolished the inactivation-permitting activity which could be re-established in the presence of a reducing agent (GSH or TCEP) (Fig. 13).

These results indicated that the cytosolic factor necessary to inhibit GPx4 activity by 1*S*,3*R* RSL3, is redox sensitive.

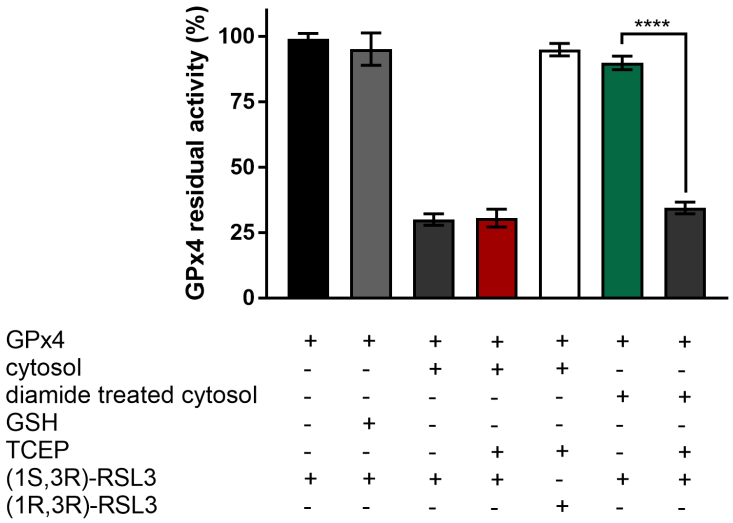

Figure 13. Diamide restricts the inactivation-permitting activity of cytosol, and this effect can be reversed by a reducing agent

50 nM of purified GPx4 and 0.5 mg/mL of HEK293T cytosol proteins were used. Where indicated, cytosol was treated with 10 mM diamide which was further freed from the thiol oxidizing agent prior to use. Where indicated, 100 µM of RSL3 stereoisomer was used. When present, GSH or TCEP concertation was 2.5 mM. Results are expressed as the percentage of residual GPx4 activity. Data are presented as mean ± SD from n=3 independent experiments. All quantitative data are presented as mean ± SD of n=3 experiments (****$p < 0.0001$, one-way ANOVA).

3.2.1. 14-3-3 proteins account for the inactivation-permitting activity of cytosol on GPx4 induced by RSL3

Aiming to unravel the mechanism of GPx4 inactivation and the nature of the redox sensitive cytosolic factor we resorted to purify it. Using the inhibition permitting activity to follow purification steps we progressively increased the specific activity of HEK293T cell cytosol by ion exchange chromatography and size exclusion chromatography. The most active fractions were analysed by MS/MS. Based on exponentially modified protein abundance index (emPAI), we identified prothymosine α and 14-3-3 isoforms as the most abundant proteins. We also carried out in parallel the purification process on rat kidney cytosol.

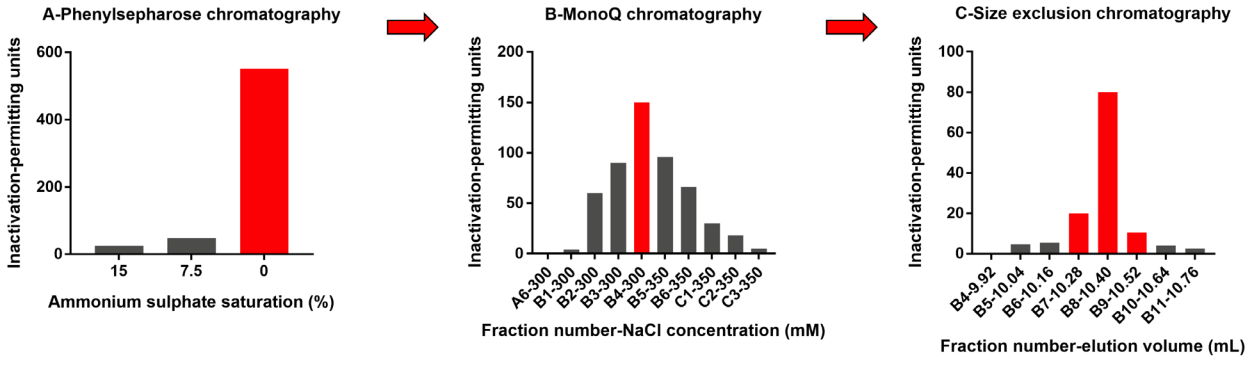

Figure 14. Purification scheme for the protein permitting GPx4 inactivation by RSL3
GPx4 inactivation-permitting activity was purified from rat kidney cytosol by a three-step chromatographic process: (A) hydrophobic interaction chromatography (B) ion exchange chromatography and (C) size exclusion chromatography. The red columns indicate the fractions containing the highest amount of inactivation-permitting activity used in the forthcoming step.

MS analysis confirmed the abundance of 14-3-3 isoforms and tropomyosin α, but not prothymosine in the active fractions. Thus, we implemented purification step by hydrophobic interaction, ion exchange and size exclusion chromatography (Fig. 14). Indeed, 14-3-3 isoforms ε, β/α, γ and τ had the highest identification score (Fig. 15).

Fraction B7, 10.28 mL of size exclusion chromatography

Protein_Family	Accession	Score	Mass (Da)	Matches	Sequences	emPAI	Protein name
2,1	K1C10_RAT	370	56470	23 (15)	9 (8)	0,76	Keratin, type I cytoskeletal 10 OS=Rattus norvegicus GN=Krt10 PE=3 SV=1
1,1	K2C1_RAT	371	64791	14 (11)	8 (7)	0,64	Keratin, type II cytoskeletal 1 OS=Rattus norvegicus GN=Krt1 PE=2 SV=1
4,1	1433Z_RAT	173	27754	16 (5)	5 (3)	0,57	14-3-3 protein zeta/delta OS=Rattus norvegicus GN=Ywhaz PE=1 SV=1
1,3	K2C5_RAT	196	61788	34 (9)	11 (6)	0,44	Keratin, type II cytoskeletal 5 OS=Rattus norvegicus GN=Krt5 PE=1 SV=1
4,2	1433T_RAT	118	27761	12 (4)	3 (2)	0,41	14-3-3 protein theta OS=Rattus norvegicus GN=Ywhaq PE=1 SV=1
9	HSBP1_RAT	43	8579	4 (3)	2 (1)	0,41	Heat shock factor-binding protein 1 OS=Rattus norvegicus GN=Hsbp1 PE=3 SV=1
4,3	1433B_RAT	41	28037	15 (3)	4 (2)	0,4	14-3-3 protein beta/alpha OS=Rattus norvegicus GN=Ywhab PE=1 SV=3
7	1433E_RAT	52	29155	5 (3)	4 (3)	0,38	14-3-3 protein epsilon OS=Rattus norvegicus GN=Ywhae PE=1 SV=1

Fraction B8, 10.40 mL of size exclusion chromatography

Protein_Family	Accession	Score	Mass (Da)	Matches	Sequences	emPAI	Protein name
2,1	1433E_RAT	430	29155	32 (22)	13 (10)	4,05	14-3-3 protein epsilon OS=Rattus norvegicus GN=Ywhae PE=1 SV=1
2,2	1433B_RAT	303	28037	52 (18)	14 (10)	3,29	14-3-3 protein beta/alpha OS=Rattus norvegicus GN=Ywhab PE=1 SV=3
2,3	1433G_RAT	297	28285	31 (16)	11 (9)	2,4	14-3-3 protein gamma OS=Rattus norvegicus GN=Ywhag PE=1 SV=2
2,4	1433T_RAT	283	27761	37 (13)	9 (7)	1,48	14-3-3 protein theta OS=Rattus norvegicus GN=Ywhaq PE=1 SV=1

Fraction B9, 10.52 mL of size exclusion chromatography

Protein_Family	Accession	Score	Mass (Da)	Matches	Sequences	emPAI	Protein name
3,1	1433Z_RAT	341	27754	19 (12)	11 (9)	2,48	14-3-3 protein zeta/delta OS=Rattus norvegicus GN=Ywhaz PE=1 SV=1
1,2	K2C5_RAT	861	61788	63 (45)	22 (18)	2,29	Keratin, type II cytoskeletal 5 OS=Rattus norvegicus GN=Krt5 PE=1 SV=1
2,1	K1C10_RAT	827	56470	51 (33)	18 (12)	1,93	Keratin, type I cytoskeletal 10 OS=Rattus norvegicus GN=Krt10 PE=3 SV=1
2,2	K1C14_RAT	525	52651	34 (22)	14 (11)	1,64	Keratin, type I cytoskeletal 14 OS=Rattus norvegicus GN=Krt14 PE=2 SV=1
3,2	1433B_RAT	221	28037	14 (9)	7 (5)	1,45	14-3-3 protein beta/alpha OS=Rattus norvegicus GN=Ywhab PE=1 SV=3
1,1	K2C1_RAT	989	64791	40 (36)	10 (10)	1,21	Keratin, type II cytoskeletal 1 OS=Rattus norvegicus GN=Krt1 PE=2 SV=1
3,5	1433E_RAT	159	29155	11 (7)	9 (5)	1,13	14-3-3 protein epsilon OS=Rattus norvegicus GN=Ywhae PE=1 SV=1
2,3	K1C17_RAT	488	48093	29 (20)	14 (10)	1,08	Keratin, type I cytoskeletal 17 OS=Rattus norvegicus GN=Krt17 PE=1 SV=1
3,3	1433T_RAT	200	27761	13 (7)	8 (5)	0,97	14-3-3 protein theta OS=Rattus norvegicus GN=Ywhaq PE=1 SV=1
3,4	1433G_RAT	174	28285	6 (6)	5 (5)	0,95	14-3-3 protein gamma OS=Rattus norvegicus GN=Ywhag PE=1 SV=2

Figure 15. 14-3-3 proteins account for the inactivation-permitting activity
MS analysis of fractions B7, B8 and B9 obtained after the last chromatographic step.

3.2.2. Recombinant 14-3-3ε permits GPx4 inactivation by RSL3

To validate our results obtained by MS identification, we used bacterially expressed and purified recombinant 14-3-3ε. Then, we tested whether recombinant 14-3-3ε could substitute for cell cytosol in our assay allowing the inactivation of GPx4 by RSL3. Indeed, recombinant 14-3-3ε permits the inactivation of GPx4 by 1*S*,3*R* RSL3 while the diastereomer 1*R*,3*R* RSL3 was inactive (Fig. 16)

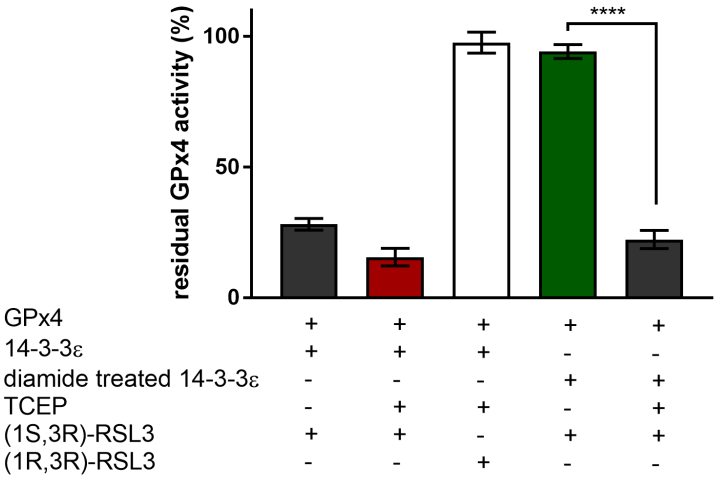

Figure 16. Only reduced 14-3-3ε permits the inactivation of GPx4 by 1S,3R RSL3
Both, GPx4 and recombinant 14-3-3ε were reduced and liberated from thiol prior to use. Each sample was divided in two parts and incubated with 100 µM of the specified diastereomer or solvent. Diamide (10 mM) treated 14-3-3ε (0.5 µM) was liberated from the compound before use. Where indicated, TCEP concentration during the inactivation test was 2.5 mM. The results are expressed as the percentage of residual GPx4 activity in treated samples and are the mean and the standard deviation of the mean of three independent experiments (****p < 0.0001, one-way ANOVA).

During the purification process, recombinant 14-3-3ε was kept in the presence of a thiol and prior to use in inactivation assays it was liberated from it by buffer exchange. Under these conditions the protein maintains its ability to permit the inactivation of GPx4 by RSL3 for several hours. As observed using cell cytosol, diamide abolished also the inactivation-permitting activity of recombinant 14-3-3ε, which could be re-established in the presence of a disulphide reducing agent (Fig. 16). Furthermore, the inactivation was dependent on 14-3-3ε and RSL3 concentration (Fig. 17)

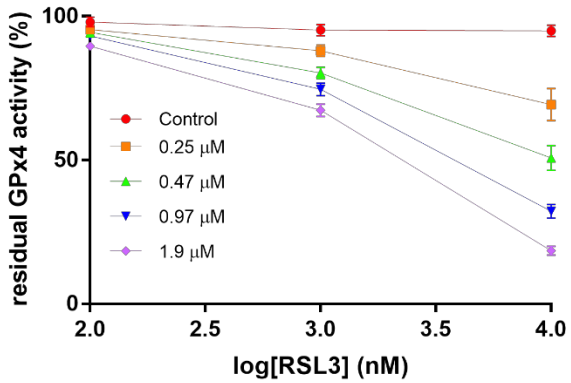

Figure 17. Gpx4 inactivation by RSL3 depends on 14-3-3ε and RSL3 concentration
Aliquots of purified GPx4 (50 nM) with different concentrations of reduced recombinant 14-3-3ε (various concentrations are indicated with different colors) were prepared and incubated with different RSL3 concentrations or solvent for 20 minutes. The results are expressed as percentage of the residual activity of RSL3-treated vs blank sample. Data are presented as mean and standard deviation of n=3 experiments.

3.2.3. Selenocysteine is essential for RSL3 inactivation of GPx4

Next, we tested whether RSL3 in the presence of reduced 14-3-3ε actually binds to the catalytic site of GPx4. In fact, MS analysis revealed that RSL3 is covalently bound the selenium in the active site of GPx4 (Fig. 18). This indicates a nucleophilic substitution reaction, where Cl^- is the leaving group. These data validated the previously described mechanism based on the notion that the electrophilic chloroacetamide moiety of RSL3 reacts with the nucleophilic selenium of GPx4.

A

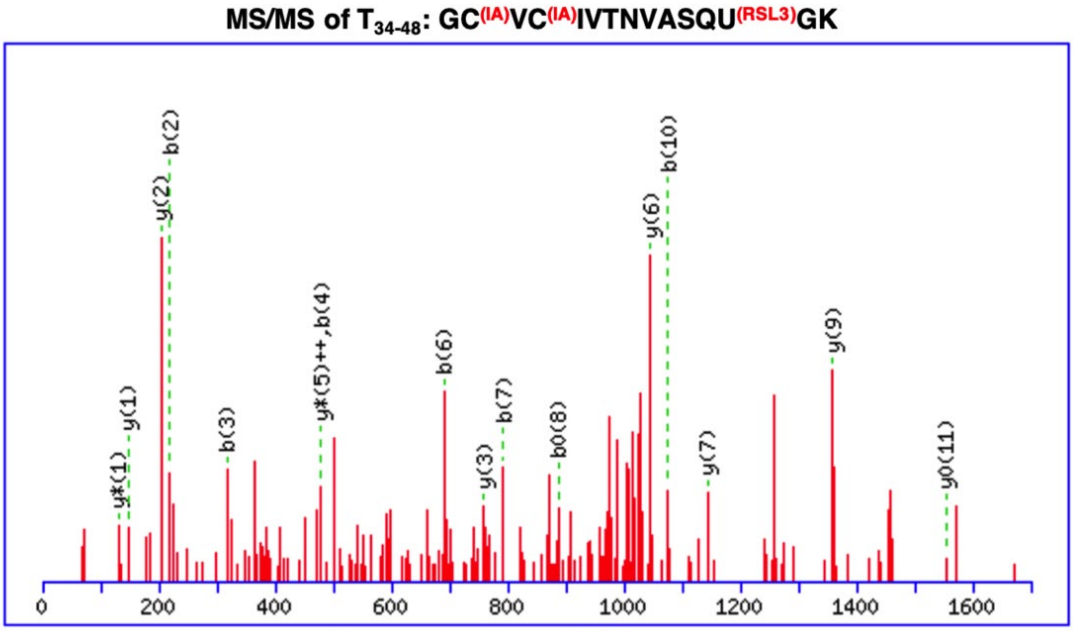

B

#	b	b^{++}	b*	b^{*++}	b^0	b^{0++}	Seq.	y	y^{++}	y*	y^{*++}	y^0	y^{0++}	#
1	58.0287	29.5180					G							15
2	*219.0434*	110.0253					C	1992.7621	996.8847	1975.7355	988.3714	1974.7515	987.8794	14
3	*318.1118*	159.5595					V	1831.7474	916.3773	1814.7209	907.8641	1813.7369	907.3721	13
4	*479.1265*	240.0669					C	1732.6790	866.8431	1715.6525	858.3299	1714.6684	857.8379	12
5	592.2105	296.6089					I	1571.6643	786.3358	1554.6378	777.8225	1553.6538	777.3305	11
6	*691.2790*	346.1431					V	1458.5803	729.7938	1441.5537	721.2805	1440.5697	720.7885	10
7	*792.3266*	396.6670			774.3161	387.6617	T	*1359.5119*	680.2596	1342.4853	671.7463	1341.5013	671.2543	9
8	906.3696	453.6884	889.3430	445.1751	888.3590	444.6831	N	1258.4642	629.7357	1241.4376	621.2225	1240.4536	620.7304	8
9	1005.4380	503.2226	988.4114	494.7094	987.4274	494.2173	V	*1144.4213*	572.7143	1127.3947	564.2010	1126.4107	563.7090	7
10	*1076.4751*	538.7412	1059.4485	530.2279	1058.4645	529.7359	A	*1045.3528*	523.1801	1028.3263	514.6668	1027.3423	514.1748	6
11	1163.5071	582.2572	1146.4806	573.7439	1145.4966	573.2519	S	974.3157	487.6615	957.2892	479.1482	956.3052	478.6562	5
12	1291.5657	646.2865	1274.5392	637.7732	1273.5551	637.2812	Q	887.2837	444.1455	870.2571	435.6322			4
13	1846.6566	923.8319	1829.6300	915.3186	1828.6460	914.8266	U	*759.2251*	380.1162	742.1986	371.6029			3
14	1903.6780	952.3426	1886.6515	943.8294	1885.6675	943.3374	G	*204.1343*	102.5708	187.1077	94.0575			2
15							K	*147.1128*	74.0600	130.0863	65.5468			1

Figure 18. Selenocysteine in the catalytic site of GPx4 is alkylated by RSL3
Reduced 14-3-3ε and GPx4 were incubated in the presence of 100 µM RSL3 for 20 minutes before carboxymethylation and hydrolysis. Tryptic fragments were analyzed by MS/MS.
(A) Tandem mass spectrum of the fragment corresponding to T34-48 tryptic peptide harboring one RSL3 species and two carboxymethylation.
(B) The identified sequence GC(IA)VC(IA)IVTNVASQU(RSL3)GK, shows SeCys46 covalently bound to RSL3 and carboxymethylation on Cys35 and Cys37.

3.2.4. GPx4 interacts with reduced 14-3-3 in the absence of RSL3

Given that we found that GPx4 is inactivated by RSL3 in the presence of reduced 14-3-3ε, we wanted to examine if a protein-protein interaction between 14-3-3ε and GPx4 occurs. In order to test this, we used biotin as an affinity tag on reduced 14-3-3ε. Of note, biotinylation of 14-3-3ε did not interfere with the capability of the protein to permit the inhibition of GPx4 by RSL3. Thus, we incubated 14-3-3ε with GPx4 in the presence or absence of RSL3. We observed that streptavidin linked to magnetic beads captured biotinylated 14-3-3ε/GPx4 complex only in the absence of RSL3 treatment (Fig. 19A, lane 1). On the contrary, in the presence of RSL3 no interaction was observed (Fig 19A, lane 2). The interaction was also confirmed using biotinylated 14-3-3ε and endogenous GPx4 present in HEK293T cytosol (Fig. 19B). This result indicates that the interaction between 14-3-3ε and GPx4 is independent from RSL3 and that the reaction of RSL3 with the active selenocysteine reverts the interaction.

To further evaluate our results of interaction of 14-3-3 and GPx4, we used HEK293T cell cytosol containing biotinylated GPx4 and observed that it binds 14-3-3 proteins present in the cell cytosol (Fig. 19C).

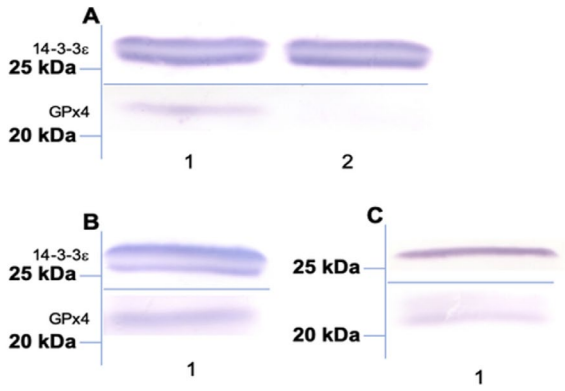

Figure 19. GPx4 interacts with 14-3-3ε

(A) Biotinylated 14-3-3ε and purified GPx4 are pulled down together (lane 1) in absence of RSL3 treatment. The treatment of 200 μM RSL3 inhibits the interaction (lane 2).
(B) Biotinylated 14-3-3ε binds GPx4 present in cell cytosol (lane 1).
(C) Biotinylated GPx4 binds 14-3-3 proteins of cell cytosol (lane 1)

14-3-3 proteins are involved in several cellular processes, such as signal transduction, protein trafficking and apoptosis. They are adaptor proteins known to assist in protein folding, stimulating or inhibiting other interactions. Thus, we performed a bioinformatic analysis using 14-3-3Pred tool which can predict a putative binding motif of the target protein. In fact, 14-3-3Pred tool indicates a (DWRCAR^{13}SMHEF) 14-3-3 binding motif in GPx4. However, as there is no evidence for

phosphorylation of ^{13}S in purified GPx4 by MS analysis, and our inhibition assay can be performed in phosphate buffer we feel confident ruling out a role of phosphorylation in the protein-protein interaction. Furthermore, GPx4 doesn't contain any structural elements on the surface that can fit the amphipathic groove on 14-3-3 proteins typically required for binding to its targets. The formation of a seleno-disulfide between 14-3-3 and the catalytic Sec is also excluded as the inactivation-permitting activity can be observed also in the presence of millimolar GSH. Moreover, we observed that a high ionic strength decreases the permitting activity of 14-3-3ε on GPx4 inactivation by RSL3, strongly suggesting that it is just an electrostatic interaction taking place among the two proteins.

3.2.5. GPx4 kinetics is not affected by 14-3-3 interaction

To unravel whether the interaction between 14-3-3ε and GPx4 impacts on GPx4 protein dynamic during catalysis, we calculated the rate constants of the peroxidatic and reductive steps of GPx4 reaction under steady state conditions in the presence of 14-3-3ε. Second order rate constants were measured according to Ursini et al.[28].

As indicated in Table 2., kinetic constants did not change in the presence of 14-3-3ε.

	GPx4		GPx4/14-3-3 ε	
	mean (M^{-1} s^{-1})	**st.dev.** (M-1 s^{-1})	**mean** (M^{-1} s^{-1})	**st.dev.** (M^{-1} s^{-1})
k_{+1}	1.51 x 10^7	0.38 x 10^7	1.38 x 10^7	0.11 x 10^7
k_{+2}	7.57 x 10^7	0.94 x 10^7	7.26 x 10^7	2.13 x 10^7

Table 2. GPx4 kinetics is not affected by 14-3-3ε
Rate constants were calculated by the Dalziel equation (see Materials and Methods) where k_{+1} and k_{+2} are the Dalziel coefficients, equivalent to the reciprocal of the second order rate constant of the oxidative and reductive steps of the reaction, respectively.

3.2.6. Overexpression or silencing of 14-3-3ε affects inactivation-permitting activity in the cytosol

We first transiently transfected HEK293T with pcDNA3.1. vector containing human 14-3-3ε and with the empty vector for controls. Overexpression was confirmed by immunoblotting (Fig.20A). GPx4 inactivation by RSL3 was measured using three different protein concentration of cell cytosols and four RSL3 concentrations.

A significant difference was already detected using 1 µM RSL3 and 1.14 mg/mL protein, as well as 2.28 mg/mL protein in cells overexpressing 14-3-3ε. Furthermore, using 10 µM RSL3 a more persistent inhibition of GPx4 was observed at all the protein concentrations used (Fig. 20B).

Consistent with the foregoing results, silencing of YWHAE, gene coding for 14-3-3ε, decreased the efficiency of cytosol in inhibiting GPx4 in the presence of RSL3 in respect to control (scrambled) cells (Fig. 20C and D). Again, in this experiment, three different protein concentrations were tested using 100 µM RSL3. A significative difference was obtained with 0.25 and 0.5 mg/mL, while no significant difference was observed with the lowest protein concentration used, 0.1 mg/mL.

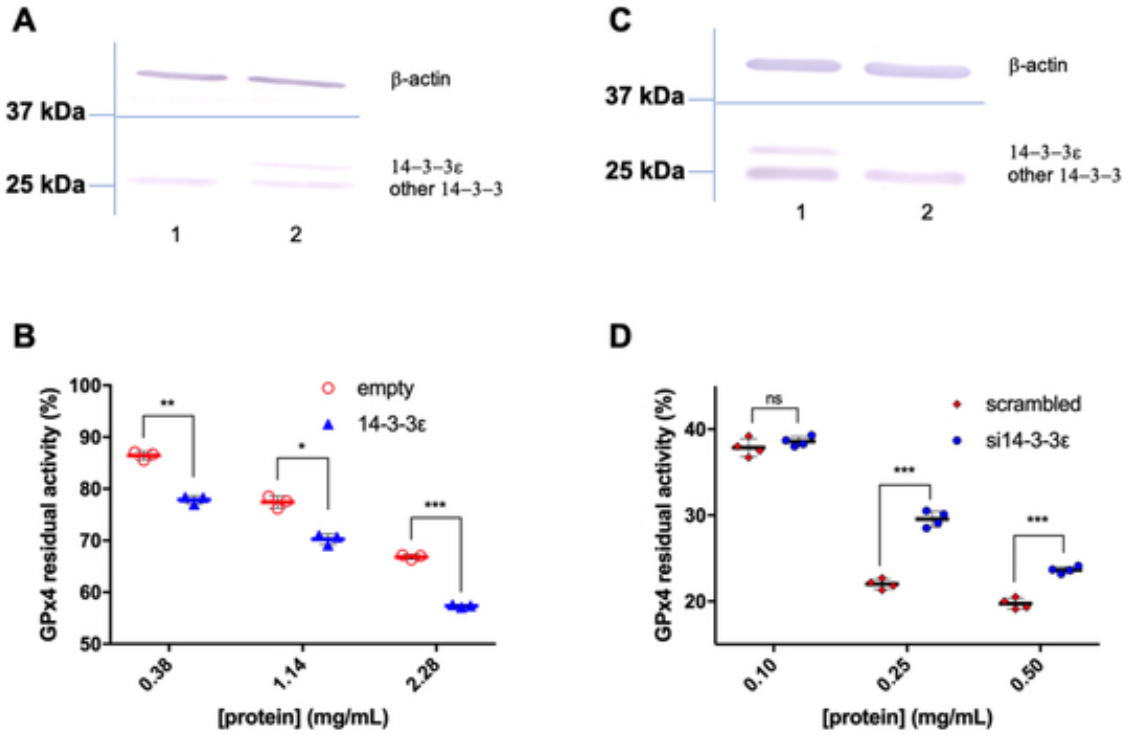

Figure 20. Modulation of 14-3-3 expression in HEK293T cells affects the inactivation permitting activity of the cell cytosol

(A) Overexpression of 14-3-3ε in HEK293T cells was verified by immunoblotting.
(B) GPx4 inactivation is more sensitized in 14-3-3ε overexpressed HEK293T cells. Purified GPx4 was added to different protein concentrations of cytosol transfected with the empty vector (red circles) or with vector containing 14-3-3ε (blue triangles) and then treated with 10 µM RSL3.
(C) Silencing of YWHAE gene was confirmed by immunoblotting.
(D) Lower GPx4 inactivation was measured with 0.25 and 0.5 mg mL-1 si14-3-3ε HEK293T cell cytosol. GPx4 was incubated with 100 µM RSL3 with different protein concentrations from cytosol of control HEK293T cells (red diamonds) and si14-3-3ε HEK293T cells (blue circles). Data are presented as mean and standard deviation of the mean of three and four replicates for overexpression and silencing experiments, respectively (* $p<0.01$; ** $p<0.001$ and *** $p<0.0001$, one-way ANOVA)

Given the observation that 14-3-3ε overexpression fosters inhibition of GPx4 activity by RSL3, we carried out experiments with HEK293T cells overexpressed or silenced with 14-3-3ε to verify the

impact on ferroptosis. Unfortunately, our experiments led to inconclusive results that might be justified by compensatory mechanisms and the intervention of other 14-3-3 isoforms.

In this part of the study we found that 14-3-3ε is indispensable to GPx4 inactivation by RSL3. Hence, our results corroborate the notion that the inhibition of GPx4 can be seen as a regulated event encompassing cellular redox homeostasis essential for cell life and death decisions. In this scenario, unfortunately, we don't know so far what could be the physiological electrophile mimicking the activity of RSL3.

14-3-3 proteins are involved in many cellular processes interacting with proteins. There are seven mammalian isoforms of 14-3-3 (α/β, γ, δ/ζ, ε, τ, σ, and η) that form homo- and heterodimers. As these isoforms can complement each other in performing their function, this could give an account for failure of experiments when modulation of the expression of 14-3-3 epsilon was tested in relation to cell death.

The feature of protein-protein interaction is compatible with a conformational shift of GPx4 induced by 14-3-3, which is permissive of the inhibition of the enzyme by RSL3. At the same time alkylation of Sec -and possibly other Cys residues- contributes to other conformational changes that weakens the affinity for 14-3-3. This discloses 14-3-3 as the scaffold permitting inactivation of GPx4.

Our data also unravel the notion of a redox regulation of 14-3-3. The inhibitory electrophile, indeed, can alkylate the catalytic Sec and inactivate GPx4 only following the interaction with the adaptor protein 14-3-3 in the reduced form. This observation fits with the already known redox regulation of these proteins. The inhibition of GPx4 is prevented by formation of a disulfide in 14-3-3. This is reminiscent of a feedback homeostatic regulation where a reduced nucleophilic tone contributes to resistance to ferroptosis by protecting GPx4 against inactivation by an electrophile. The other way around, a nucleophilic environment would favour the inactivation of the peroxidase and thus the execution of cell death by an electrophile. In summary, the evidence about redox regulation of 14-3-3ε brings to the focus the challenging option of a redox control of the inactivation of this vital enzyme. On this light, our data are indicative of a complex homeostatic regulation of cell life and death decision of which GPx4 is the final master regulator.

4. CONCLUSIONS AND PERSPECTIVES

The identification of ferroptosis as a form of cell death operated by lipid peroxidation and descending from missing GPx4 activity, brought a substantial contribution to the accurate definition of "regulated cell death". Differently from "programmed cell death", (the prototype of which is apoptosis), ferroptosis is not activated by a specific agonist activating a specific signal transduction pathway. Instead, lipid peroxidation, the actual event leading to ferroptosis, is activated in the frame of regular oxidative metabolism, when formation of oxidatively modified lipids overwhelms the critical counteracting mechanism.

In this perspective, several constraints must be fulfilled on order to reach a breakeven point when the critical reduction of PL-OOH is not anymore sufficient to prevent lipid peroxidation.

In a broad sense, therefore, it is oxygen toxicity itself that is competent for killing cells in a regulated manner. Oxygen, indeed, besides its function in bioenergetics, and having been also described as an "environmental poison" by Lars Ernster 40 years ago[120], reveals today an unexpected physiological function descending form its toxicity. Basic chemical events, indeed, are assumed the same that led to a modification the life on the whole planet when the survival in the presence of oxygen become restricted to species that built up an efficient antioxidant system.

It is a widely accepted notion that aerobic life was made possible by the evolution of a complex multi-level anti-oxidant machinery. We know enzymes competent for dismutation of superoxide and hydrogen peroxide (SOD and catalase) and for the reduction of hydrogen peroxide (peroxidases and peroxiredoxins). We also know, however, that none of these "antioxidant enzymes" is vital. Basically, they contribute to increase the resistance to oxidative challenges. The free radical scavengers, as well, have a minimal role. Although life requires free radicals that can be also, as initially pointed out by Albert Szent-Györgyi, rather toxic, "free radical scavenging deficiency disease" has never been observed, at least in terms of the on/off control of cell death or survival.

The synthesis of GSH and the activity of GPx4, instead, are vital, and the absence of alternative mechanisms rescuing missing GPx4 reaction, is strongly indicative of a specific univocal function operated by an on/off mechanism. These concepts underscore the basic notion that what is vital is not the scavenging of free radicals initiating lipid peroxidation but the prevention of their formation by reduction of PL-OOH.

Provided the fulfilment of indispensable constraints, the switch-off of the activity of GPx4 in an aerobic cell invariably leads to cell death. In this respect it is also worth to remind that it is GPx4 activity that accounts for an indispensable role of traces of selenium in animals. In other words, the main reason why selenium is indispensable to life is the anti-peroxidant (*i.e.* anti-ferroptotic) activity of GPx4.

What is not known is the precise series of events leading to the metabolic shift evolving to the missing GPx4 activity.

A series of constraints outlines the boundaries of the cellular status compatible with activation of ferroptosis. Oxygen, polyunsaturated lipids and iron in the labile pool are necessary. Lipid peroxidation primed missing GPx4 activity is executing.

In this study we brought our contribution to the area of ferroptosis disclosing two new players in the scenario: i) a major source (possibly unique) of PL-OOH required for the initiation of lipid peroxidation; and ii) the nature and function of a scaffold protein, indispensable to inhibition of GPx4 by an electrophile.

The phases of lipid peroxidation are initiation, propagation and arrest. In each phase free radicals are produced, remain constant and decrease, respectively. Since lipid peroxidation in biological systems is always inhibited by reduction of PL-OOH the necessary conclusion is that "pre-formed" PL-OOH are indispensable to initiation. The presence of traces of PL-OOH, is not directly associated to initiation of peroxidative chain reactions, but is, instead, an indispensable constraint of ferroptosis.

As a matter of fact, also 12/15-lipoxygenase produces PL-OOH, but this does not contribute to clarify the issue of the formation of the initiating PL-OOH since hydroperoxides are also indispensable to activate the enzyme. Therefore, the most suitable role of 12/15-lipoxygenase is multiplication of PL-OOH from which lipid peroxidation is initiated, and this further underscore the critical role of GPx4 controlling both, 12/15-lipoxygenase activity and lipid peroxidation.

The formation of PL-OOH requires a free radical oxidant and an H transfer to stabilize the oxygen addiction to the radical.

Our evidence that mitochondrial oxidation of α-keto acids, but not respiratory chain, is indispensable to ferroptosis primed by GSH depletion, contributes to bridge the gap between mitochondrial activity and ferroptosis.

It has been already convincingly shown that α-keto acid dehydrogenases are the major source of superoxide anion in mitochondria and we now achieved non-ambiguous evidence that is also an

indispensable constraint of ferroptosis. The most reasonable mechanism, in agreement with basic chemistry of lipid peroxidation, is that an extremely tiny amount of superoxide in protonated form, escaping enzymatic dismutation, could be competent for the H abstraction in the methylene bridge of polyunsaturated fatty acids forming of the carbon centered radical. The oxygen addiction is then stabilized by a coenzyme Q, the most suitable and available species donating H this reaction.

As a suitable alternative it is hydrogen peroxide escaping reduction that could activate 12/15-lipoxygenase, although this has never been positively demonstrated.

Formation of PL-OOH is not sufficient to initiate chain reaction. The traces of PL-OOH, indeed, initiate lipid peroxidation only in the presence of ferrous iron and, obviously, only when GPx4 activity is missing. Traces of PL-OOH, therefore, must be rated as a constraint of ferroptosis as unavoidable consequence of respiration.

Hydrolysis of hydroxy fatty acids and re-acylation of lysophospholipids are assumed to complete the continuous repair of the membrane. The notion of the existence of such a continuous repair mechanism is indirectly supported by the existence of a specific syndrome where the pathological phenotype is accounted by missing re-acylation of cardiolipins in mitochondria, the lipid most prone to peroxidation.

The other constraint of ferroptosis disclosed in this study is that GPx4 can be inhibited by RSL3 only in the presence of a 14-3-3, seemingly playing a role of scaffold protein operating by conformational switches in GPx4. Moreover, this activity 14-3-3 is redox regulated, being GPx4 inactivation possible only when a disulphide in 14-3-3 is reduced.

The biologically relevant notion suggested by this result is that GPx4 undergoes functional conformational switches, controlled by a redox sensitive scaffold protein, impacting on its sensitivity to electrophiles of which RSL3 is reasonably just a pharmacological mimetic.

This is critical and innovative aspect worth of an in deep analysis in the future.

Cumulatively, the two players in the control of ferroptosis identified and discussed in this dissertation further contribute to frame ferroptosis in a physiological framework.

Ferroptosis is seen as a player of tissue homeostasis where the death mechanism operates by toxicity of oxygen. It is the couple iron-oxygen and the associated electron transfer reactions that provide the common soil of large part of the biology and toxicity of oxygen.

Consistently, it is not surprising that proliferating, energy and oxygen utilizing cells are those most susceptible to ferroptosis. Indirectly, this dual nature emerges as a possibly relevant feedback control of proliferation.

It is stimulating recalling in this perspective that the Warburg effect, shifting the metabolism from mitochondria to glycolysis, would favour tumour growth also by decreasing the susceptibility to ferroptosis.

The most relevant missing critical aspect is the control of GSH concentration. In the most simplistic way, it is reasonable assuming that GSH content in cells is distributed in a Gaussian and that the lower level is associated to higher sensitivity to ferroptosis that is executed when metabolic need increases the challenge. Although already suggested by compelling experimental evidence[121], this concept requires more specifically addressed studies.

From the whole set of available information, including our results, we can view at ferroptosis as an indispensable component of the life and death dualism in a thermodynamic perspective. Death is the consequence of a decreased capability of a cell to maintain the necessary continuous decrease of entropy. In this respect, the control of peroxidative degradation of membranes, indeed, fits the notion of life supported by negative entropy proposed by Erwin Schrödinger.

"*...entropy, taken with negative sign, is itself a measure of order. Thus the device by which an organism maintains itself at a fairy high level of orderliness (low entropy) really consists in continually sucking orderliness from the environment*"… (Erwin Schrödinger, What is life, 1943).

The energy requiring prevention of lipid peroxidation, preserving order in membranes (low entropy), permits aerobic life. Abating this control unchains oxygen toxicity that increases disorder in membranes (high entropy) leading to death by loss of a fundamental function.

Also, in this perspective ferroptosis is a fundamental component of aerobic life.

5. MATERIALS AND METHODS

Cell cultures and reagents

HT1080 cells (ATCC® CCL 121™) were cultured in DMEM, low glucose, 4 mM Gln, 1 mM Sodium Pyruvate (Gibco) containing containing 10% (v/v) FBS, 1% (v/v) penicillin/streptomycin. Where indicated, Gln was substituted with various concentrations of Sodium Pyruvate (Sigma-Aldrich), Sodium 2-oxobutyrate (Sigma-Aldrich), Dimethyl 2-oxoglutarate (Sigma-Aldrich) and treated immediately with erastin (Selleckchem) or RSL3, a generous gift from Dr. B.R. Stockwell.

HEK293T cells (ATCC® CRL-3216™, generous gift of Prof. S. Piccolo, University of Padova) were cultured in DMEM, high glucose, GlutaMAX™ supplement (Gibco) containing 10% (v/v) FBS, 1% (v/v) penicillin/streptomycin.

Cell counting with Neubauer chamber

To determine the necessary cell density, cells were trypsinized for 5 minutes at 37˚C, centrifuged at 250 x g and the obtained cell pellet was resuspended in 10 mL of culture media. 100 µL of the suspension was mixed 1:3 with 0.4% Trypan Blue Solution (Sigma Aldrich) to stain for dead cells. Using a Neubauer chamber number of viable cells was determined.

Measurement of mitochondrial consumption rate

Seahorse Bioscience Extracellular Flux Analyzer

Oxygen consumption rates were determined using a Seahorse Bioscience Extracellular Flux Analyzer (XF24-3). Cells were plated in Seahorse Bioscience 24 well plates (35 000 cells/well in 600 µl complete DMEM) and allowed to attach overnight. The following day cells were washed 2 times in Seahorse XF DMEM Medium, pH 7.4 assay media (Agilent Technologies) before treatment. Oxygen consumption measurements were compared between basal measurements and measurements following injection of the FCCP, rotenone or antimycin. After measurements, mitochondrial oxygen consumption rates were normalized with relative fluorescence units (RFU) of cells incorporating Calcein AM (Invitrogen™). Fluorescence was recorded using 490 nm excitation filter and a 520 nm emission filter. The fluorescence intensity is proportional to the number of viable cells.

MitoXpress

The cellular OCR was measured using the Oxygen Consumption assay MitoXpress® Xtra- (Agilent). HT1080 cells were seeded at low (15 000/well) and high (60 000/well) density in a 96 wells plate (Eppendorf), avoiding outside wells and filling with 5 mL PBS the moat.

The day after, the medium was replaced with 100 µL mixture containing 90 µL prewarmed DMEM (without red phenol and FBS, buffered with 20 mM HEPES, pH 7.4) and 10 µL reconstituted MitoXpress® Xtra reagent. The wells were sealed by adding 100 µL of prewarmed HS mineral oil.

Fluorescence decay was measured kinetically in a microplate reader (EnVision - PerkinElmer) at 37°C in time-resolved fluorescence (TR-F) mode using a filter set as follows, 380 nm excitation and 620 nm emission filters, window time 100 µs, delay 40 µs.

At the end of each experiment, the correct cell number was evaluated with Calcein AM (Invitrogen™).

Cell viability

Cells were seeded onto a 96-well plate (3000 cells/well) and treated with indicated compounds. Cell viability was assessed at different time points after treatment using resazurin sodium salt (Sigma-Aldrich). Upon entering living cells, resazurin is reduced to fluorescent resorufin. Fluorescence was measured by FluoScan (ThermoSystem, ex. 544 nm ±15, em. 590±14 nm) where resazurin reduction rate was evaluated as A.F.U/min and expressed as % vs. control.

Determination of total GSH (Tietze assay)

Cells were seeded onto a 6-well plate (150 000 cells/well) and cultured for 24h. After treatment, cells were washed with PBS and lysed in buffer containing 0.1 M KH2PO4/K2HPO4, 0.15 M KCl, 0.05% CHAPS pH 7 and protease inhibitors.

GSH was measured using an enzymatic method in which GSH reacts with 5-5'-dithiobis [2-nitrobenzoic acid] (Sigma-Aldrich) forming the 5-thionitrobenzoic acid that can be quantified spectrophotometrically at 412 nm. Any GSSG in the sample is reduced by NADPH and glutathione reductase (Sigma-Aldrich). The reaction was started by adding 10 µL of the sample in buffer containing 0.1 M NaH_2PO_4/Na_2HPO_4 pH 7.4, 1 mM EDTA, 0.14 mM DTNB, 0.1 mM NADPH and 0.8 units/mL of glutathione reductase. Total glutathione is quantitated referring to a standard curve.

Lipid peroxidation measurement

Cells were seeded onto a 6-well plate (150 000 cells/well) and the next day treated as indicated. Cells were incubated for 60 minutes with 1 µM BODIPY 581/591 C11 staining (Invitrogen™) before harvesting by trypsinization. Subsequently, cells were resuspended in 300 µL PSB for flow cytometry analysis (BD, FACSCantoII™, equipped with a 488 nm excitation laser). Fluorescence of C11-BODIPY was measured 535 nm. 6 wells plates without BODIPY were monitored to allow the subtraction of auto-fluorescence. 10 000 cells were analysed per sample. Data analysis was conducted using BD FACSDiva™ Software.

Purification of GPx4

GPx4 was purified from rat testis according to Roveri et al[34]. Briefly, four chromatographic steps were used to purify GPx4: glutathione-bromosulfophtalein affinity chromatography, hydrophobic interaction chromatography, ion exchange chromatography and size exclusion chromatography. Obtained protein concentration was 0.05 mg mL^{-1} and specific activity was 130 µmol $mg^{-1}min^{-1}$ at 25°C in the presence of 2.5 mM GSH and 30 µM phosphatidylcholine hydroperoxide (PCOOH).

Substrate preparation for GPx4 activity measurements

The reaction mixture for preparing PCOOH contained 0.2M Tris-HCl pH 8.6, 3mM deoxycholate (DOC) and 0.3mM soybean phosphatidylcholine type III-S (Sigma-Aldrich), which was previously dried under an argon stream and dispersed by 10mM DOC. The reaction was started by adding 659U of soybean lipoxygenase type V (Sigma Aldrich). After approximately 20 minutes, the prepared mixture was applied to Sep-pack C-18 reverse phase cartridge (Waters-Millipore) previously washed with methanol and water. Subsequently, DOC was washed off with water and PCOOH was eluted with 2 ml of methanol.

GPx4 activity measurement

GPx4 enzymatic activity measurement was performed by a coupled spectrophotometric test using Cary 50 UV-Vis spectrophotometer (Agilent Technologies). GPx4 activity was determined at 340 nm measuring the NADPH consumption in the presence of glutathione reductase (Sigma Aldrich). The samples were mixed in 1 mL of activity assay buffer (0.1 M KH_2PO_4/K_2HPO4 pH 7.8, 0.1% Triton, 5 mM EDTA, 2.5 mM GSH, 0.16 mM NADPH and 2 U/ml glutathione reductase) and the reaction was started by using 30 µM of PCOOH. GPx4 activity was calculated using NADPH extinction coefficient εNADPH= 6.22 mM^{-1} cm^{-1}.

Preparation of cytosol used for inactivation assays

HEK293T cell cytosol was prepared using homogenizing buffer (100 mM Tris-HCl, 250 mM sucrose, pH 7.4 and protease inhibitors) by 100 strokes of a hand-held, low clearance, glass homogenizer. The prepared homogenate was centrifuged at 105 000 x *g* for 1h and the supernatant (cytosol) used for GPx4 inactivation assays.

Measurement of the activity permitting GPx4 inactivation by RSL3

Purified GPx4 was reduced with 30 mM 2-mercaptoethanol for one hour in an ice-cold bath and freed from thiol just before the experiment by buffer exchange on PD SpinTrap™ G-25 (GE Healthcare) equilibrated with 50 mM KH_2PO_4/K_2HPO_4, 1 mM EDTA, 0.05% CHAPS (w/v), pH 7.0. For an inactivation assay, 0.05 mg proteins of the prepared cytosol and 100 ng of GPx4 were diluted in 0.1 mL of homogenizing buffer. Each test sample was divided into two identical parts and treated with

0.1 mM RSL3 diastereomer or solvent. Controls were carried out by diluting GPx4 in homogenizing buffer. GPx4 activity was measured after 20 minutes of treatment at room temperature and the obtained results were expressed as the percentage of residual GPx4 activity.

For a quantitative evaluation of the inactivation-permitting activity, its units (U) were defined as follows. One U is the amount of inactivation-permitting activity yielding 50% GPx4 inactivation using: 0.05 mL of inactivation test volume, 50 ng of GPx4 (specific activity: 130 μmoles $mg^{-1}min^{-1}$), 100 μM RSL3, upon 20 minutes of time incubation at 25°C.

When using reducing agents or thiol oxidizing agents, the samples were liberated from these agents by buffer exchange on PD SpinTrap™ G-25 equilibrated with 100 mM Tris-HCl, 250 mM sucrose, pH 7.4, 0.05% CHAPS.

Purification of the inactivation-permitting protein(s)

Wide-range molecular weight separations of components of rat kidney cytosol were obtained through centrifugal concentration at different cut-off of molecular weight using Vivaspin® 500 MWCO 50000 and Vivaspin® 500 MWCO 100000 (Sartorius AG). Purification of the inactivation-permitting protein(s) was achieved by three chromatographic steps: hydrophobic interactions chromatography, ion exchange chromatography and size exclusion chromatography. All the purification steps were performed at 4°C in a ÄKTA™ pure 25 chromatographic system (GE Healthcare). The purification steps were carried out as described below.

Hydrophobic interaction chromatography

Phenyl-sepharose® CL-4B chromatography was loaded with 0.1 g rat kidney proteins in 10 mM KH_2PO_4/K_2HPO_4, 30% saturation $(NH_4)_2SO_4$ and 5 mM 2-mercaptoethanol, pH 7.0, at 1 mL min^{-1} flow rate. After washing with 150 mL of buffer, proteins were eluted by decreasing the $(NH_4)_2SO_4$ saturation to 15%, 7.5% and 0% using eluting buffer (25 mM Tris-HCl, 5 mM 2-mercaptoethanol pH 7.5). All steps were carried out at 4˚C. The obtained samples were concentrated to 0.1 mL in DiaFlo, buffered exchanged and used for assaying GPx4 inactivation by RSL3.

Ion Exchange chromatography:

MonoQ column was equilibrated with 20 mM Tris-HCl, 5 mM NaCl, 10% (v/v) glycerol, 5 mM 2-mercaptoethanol, pH 7.4 (starting buffer) and loaded with samples containing the highest permitting activity obtained from hydrophobic interaction chromatography, prior thoroughly dialyzed against starting buffer. After washing with 25 mL of starting buffer, elution was performed in a stepwise manner by increasing the ionic strength up to 1 M of NaCl (250 mM, 300 mM, 350 mM, 400 mM, 450 mM, 500 mM and 1 M). The obtained fractions were concentrated, and 0.1 mL was buffer exchanged and used for inactivation test.

Size exclusion chromatography:

Superdex™ 75 10/300 GL was equilibrated and resolved with 200 mM KH_2PO_4/K_2HPO_4, 1 mM EDTA, 0.05% (w/v) CHAPS, 1 mM GSH, pH 7.0, at 0.5 ml min^{-1} flow rate. Fractions from MonoQ chromatography containing the inactivation-permitting activity were concentrated up to 0.5 mL, buffer exchanged and finally resolved. 0.12 mL fractions were collected and 0.025 mL of each were diluted to 0.1 mL and used for inactivation test.

All chromatographic fractions to be tested for the inactivation-permitting activity were in 50 mM KH_2PO_4/K_2HPO_4, 1 mM EDTA, 2.5 mM GSH, 0.05% CHAPS (w/v), pH 7.0. When necessary to concentrate the sample, DiaFlo apparatus equipped with a YM-10 ultrafiltration membrane (Millipore) and a buffer exchange in Illustra NAP™-5 columns (GE Healthcare) were used. The inactivation assay was performed using 100 ng of purified GPx4 that was added to a 0.1 mL aliquot of the obtained fraction. Equivalent volumes were then incubated either with 100 µM mM RSL3 or solvent for 20 minutes at 25°C. After incubation, GPx4 activity was measured.

MS analysis of the fractions from size-exclusion chromatography

Fractions containing the highest inactivation permitting-activity from the size exclusion chromatography were used to identify the protein(s) by MS analysis. Samples were thoroughly dialyzed against water and brought to dryness in a Savant SpeedVac® SVC-100 concentrator (SVPT S.r.l.). Protein pellets were digested in 0.1 mL of 40 mM NH_4HCO_3, 10% (v/v) acetonitrile (ACN) containing 10 ng of Trypsin (Trypsin Gold Mass Spectrometry Grade, Promega Co) overnight at 37°C and blocked by formic acid. Trypsinized samples were dried and dissolved in 20 µl of 5% (v/v) ACN, 0.1% (v/v) formic acid aqueous solution.

Tryptic peptides were analyzed on a 1200 nano-HPLC system coupled to a 6520 Accurate-Mass Q-TOF equipped with a HPLC-Chip cube interface as nano-ESI (Agilent Technologies). Aliquots of 6 µL of the digest were trapped on a 360 nL enrichment column and resolved on a 0.075 mmx150 mm separation column packed with Polaris C18-A 3 µm material at a post-split flow rate of 300 nL min^{-1}. Peptides were eluted with a linear gradient from 0.1% (v/v) formic acid, 6% (v/v) acetonitrile : methanol (90:10) to 0.1% (v/v) formic acid, 60% (v/v) acetonitrile : methanol (90:10) in 36 min, directly on the nano ESI source.

Data were acquired with Mass Hunter Data Acquisition software, ver.B.05.00 (Agilent Technologies) in positive ion mode, in the range between 59 and 1700 m/z, at a MS and MS/MS scan rate of 3 Hz with a resolving power of 20 000 FWHM. Spray capillary voltage was set at 1.72 kV, while the ion transfer capillary temperature was held at 325 °C and drying gas to 4.8 L s^{-1}. MS/MS precursors were selected in data-dependent mode on the five most intense precursors from each scan at an isolation

width of 4 a.m.u. and fragmented by collision-induced dissociation (CID) by application of a formula weighting collision energy based on precursor charge and m/z. Raw data of MS/MS datasets were searched with Mascot search engine with an in-house server version of Mascot rev. 2.3 (Matrix Science) against the whole SwissProt database with no taxonomy restriction. Search constraints were: 10 p.p.m. tolerance for precursor ion masses and 0.05 Da tolerance for fragment ion masses. Trypsin enzyme restriction specificity was imposed for peptides, with a maximum of two missing cleavages.

Production and purification of recombinant human 14-3-3ε

pGEX-6P-1 vector containing human 14-3-3ε with the N-terminal GST was provided by GenScript USA Inc. Correctness of constructs was verified by sequencing. *Escherichia coli* BL21 pLysS was transformed with the construct. Expression was induced with 1 mM isopropyl-β-D-thiogalactopyranoside (IPTG) for 4h at 37 C, followed by harvesting of the cells by centrifugation at 5000g for 30 min at 4 C. The obtained bacterial pellet was resuspended in cold B-Per extraction reagent (Pierce, Rockford) containing 0.1 mg/ml PMSF, 0.7 mg/ml pepstatin, 0.5 mg/ml leupeptin, and stirred for 20 minutes on ice. The extraction mixture was centrifugated at 35 000 x g for 30 min. The supernatant was diluted 1:10 (v/v) with PBS (140 mM NaCl, 2.7mM KCl, 10 mM Na_2HPO_4, 1.8 mM KH_2PO_4 pH 7.3) and loaded onto a column containing GSTrap FF resin (GE Healthcare), equilibrated with the above buffer. The column was washed with 10 column volumes of the same buffer. To remove the GSTtag the column was further washed with 10 column volumes of PreScission cleavage buffer (50 mM Tris-HCl, 150 mM NaCl, 1 mM EDTA, 1 mM dithiothreitol, pH 7.5) and PreScission Protease mix: containing 160 units of PreScission Protease with 920 µl of PreScission cleavage buffer was loaded onto the column at 4 °C for 4 hours. One step elution was performed with PreScission cleavage buffer. Human 14-3-3ε obtained appeared to be 85% homogeneous on SDS–PAGE gels stained with Coomassie blue. Recombinant human 14-3-3ε was further purified by hydrophobic interactions and size exclusion chromatography.

GPx4 inactivation-permitting activity of 14-3-3ε

In all the inactivation experiments recombinant 14-3-3ε and GPx4 were previously treated with 2.5 mM GSH and 30 mM 2-mercaptoethanol, in an ice-cold bath for one hour and freed from thiol by buffer exchange on PD SpinTrap™. Preparations were used within 2-3 hours, otherwise a reducing agent (2.5 mM GSH or TCEP) was present during the inactivation assay. In a standard 0.1 mL inactivation test 50 nM GPx4 and 0.5 µM 14-3-3ε concentrations were used. The inactivation test was carried out as described for cytosol.

For experiments with diamide, recombinant 14-3-3ε in 50 mM KH_2PO_4/K_2HPO_4, 1 mM EDTA, 0.05% (w/v) CHAPS, pH 7.0 was treated with 10 mM diamide for 30 minutes in an ice-cold bath followed by a buffer exchange before performing the experiment. Briefly, GPx4 and diamide-treated 14-3-3ε were

mixed, the resulting volume was divided into equal parts and treated with either 0.1 M RSL3 or corresponding volume of the solvent. The same experiment was also performed in the presence of 2.5 mM TCEP.

Increasing concentrations of purified recombinant 14-3-3ε in 0.25 mL of 50 mM KH_2PO_4/K_2HPO_4, 1 mM EDTA, 2.5 mM GSH, 0.05% (w/v) CHAPS, pH 7.0, were mixed with fixed concentration of GPx4 (50 nM). Aliquots of each mixture were incubated with various RSL3 concentrations or solvent, for 20 minutes at 25°C. For each concentration of 14-3-3ε the percentage of residual GPx4 activity with different RSL3 concentrations was calculated based on the corresponding blank.

MS analysis of GPx4 upon incubation with RSL3 and 14-3-3ε

To search for the product of interaction between GPx4 and RSL3, reduced recombinant 14-3-3ε (0.02 mg) and rat GPx4 (0.01 mg) in 50 mM KH_2PO_4/K_2HPO_4, 1 mM EDTA, 2.5 mM GSH, 0.05% (w/v) CHAPS, pH 7.0, were incubated with 0.1 mM RSL3 for twenty minutes at 25°C. After incubation, proteins were carboxymethylated and further treated as described for chromatographic fractions before MS analysis.

MS/MS datasets were searched against ad hoc-built database for GPx4; considered variable modifications were: a) carboxymethylation on cysteine/selenocysteine, b) de-amidation on arginine/glutamine, c) RSL3 on cysteine/selenocysteine/methionine, d) dehydroalanine from selenocysteine/selenenylamide.

Kinetic constants measurement

Recombinant 14-3-3ε (0.2 μM) and GPx4 (50 nM) or GPx4 alone were diluted in 0.2 mL of 50 mM KH_2PO_4/K_2HPO_4, 1 mM EDTA, 0.05% (w/v) CHAPS, pH 7.0 containing three different GSH concentrations (2, 3, 4 mM) and incubated in an ice-cold bath for one hour. Aliquots (0.05 mL) of each mixture were tested with the same concentrations of GSH in the activity test[28]. Reactions were carried out at room temperature in activity buffer containing various GSH concentrations (2, 3, 4 mM) where 45 μM of PCOOH triggered the enzymatic reaction. In the activity test GPx4 concentration was 2.5 nM and, when present, 14-3-3ε concentration was 10 nM.

Second order rate constants of the peroxidatic and reductive steps of GPx4 reaction were measured essentially according to Ursini et al.[28]. Kinetic analysis was carried out from single progression curves of NADPH oxidation at different GSH concentrations; absorbance data *vs* time were used to calculate substrate concentration and rate at time intervals of 5 seconds. Apparent rate constants for GPx4 alone and in the presence of 14-3-3ε protein were calculated by the simplified Dalziel equation: $E/v_0 = \phi_0 + \phi_1/[PCOOH] + \phi_2/[GSH]$, where: ϕ_0 is the reciprocal of the turnover number, which for GPx4

approximates to 0, ϕ_1 and ϕ_2 are equivalent to the reciprocal of the second order rate constant of the oxidative and cumulative reductive steps of the reaction, respectively.

Protein-protein interaction assay

Reduced recombinant 14-3-3ε (12.5 μM) and GPx4 (3.5 μM) in 50 mM KH_2PO_4/K_2HPO_4, 50 mM KCl, and 0.05% (w/v) CHAPS, pH 7.0, were incubated in the presence of EZ-link™ NHS-PEG_4-Biotin reagent (Thermo Fisher Scientific) at 1:20 molar ratio, for 1 hour in an ice-cold bath followed by buffer exchange to remove the remaining free biotin.

Biotinylated 14-3-3ε and GPx4 (1.5 μg and 100 ng, respectively) in 0.1 mL were incubated with 0.2 mM RSL3 or corresponding volume of the solvent in the presence of 2.5 mM GSH, for 20 minutes at 25°C. We verified that under these conditions GPx4 was efficiently inactivated. Samples were affinity purified by reacting with 0.03 mL of streptavidin magnetic beads, 10 mg mL^{-1} (Thermo Fisher Scientific Inc) for 2-3 minutes; beads were then quickly washed three times with 0.1 mL of incubation buffer. Captured material was removed from beads with 0.04 mL of Laemmli sample buffer, at 95°C for five minutes. Controls were carried out with either non-biotinylated 14-3-3ε and GPx4 or GPx4 alone to rule out any unspecific binding to the beads. Samples were analyzed by Western Blot.

Biotinylated 14-3-3ε (1.5 μg) and biotinylated GPx4 (500 ng) were incubated with HEK293T cytosol (0.15 mg) in 50 mM KH_2PO_4/K_2HPO_4, 50 mM KCl, 2.5 mM GSH and 0.05% (w/v) CHAPS, pH 7.0 for 30 minutes at room temperature. Sample were affinity purified as reported above and used for Western Blotting.

Western blot

Proteins of cell cytosols were measured by the Bradford method using BSA as standard. Whole samples from pull-down experiments and different amounts of proteins (2.5-5 μg) for overexpression and silencing experiments were separated on a 15% Laemmli gel and blotted onto nitrocellulose overnight. Membranes were cut depending on the size of the protein of interest and blocked with 3% bovine serum albumin (BSA) in TBS (25 mM TRIS, 125 mM NaCl pH 7.4) containing 0.1% Tween for 2 hours. Anti GPx4 primary antibodies (Abcam) were used diluted 1:5000, anti 14-3-3 (pan) primary antibodies (Cell Signaling Technology) were diluted as 1:1000 and anti β-actin primary antibodies (Sigma-Aldrich) were used 1:10 000. Anti-rabbit and anti-mouse secondary antibodies Alkaline Phosphatase linked or biotin linked (Merck KGaA) were used 1:30 000 and applied for 45 minutes. Nitro-blue tetrazolium and 5-bromo-4-chloro-3'-indolyphosphate were used to detect the chromogenic signal of AP reaction. Images were acquired with Epson perfection V700 photo, dual lens system scanner.

For experiments where dihydrolipoamide dehydrogenase (DLD) was silenced, 20 µg of samples were heated to 95°C for 5 min and proteins were separated on precast NuPAGE™ 4-12% Bis-Tris Protein Gels (Invitrogen) and further transferred to a nitrocellulose membrane for Western blot analysis. After blocking with 3% bovine serum albumin (BSA) in TBS containing 0.1% Tween, anti DLD antibody (Abcam) was applied overnight. On the next day, membranes were washed three times in TBS 0.1% Tween for 10 min and horseradish peroxidase (HRP) conjugated secondary antibodies (Santa Cruz Biotechnology) were applied for 45 minutes. Membranes were washed again three times and visualized by Pierce ECL Western Blotting Substrate for HRP (Thermo Scientific™).

Silencing using Predesigned short-interfering RNA

Cells were plated at 50% of confluency in 6 wells plates after splitting and grown overnight. The next day, growth medium was changed 1 hour before the transfection into media without sera and antibiotics. For YWHAE silencing two MISSION® Predesigned short-interfering RNA (siRNA) (SASI_Hs02_00342252, SASI_Hs02_003422, Merck KGaA, Darmstadt, Germany) were used, while for DLD silencing, three predesigned siRNA (SASI_Hs01_00189500, SASI_Hs02_00301883, SASI_Hs01_00189498) were used to obtain 75% of gene silencing. To transfect, siRNAs were diluted in Opti-MEM I Reduced Serum Media (Gibco), mixed and incubated with Lipofectamine™ RNAiMAX (Invitrogen) for 15 minutes at room temperature and then added dropwise to the cells. The final concentration of RNA duplex was 30nM. The media was changed with the full growth media 24 hours post transfection. 48 hours after transfection, cells were harvested by trypsinization, washed, centrifuged and used for cytosol preparation.

For cell viability assays, 24 hours after the transfection cells were plated onto a 96-well plate (5000 cells/well) and treated the next day with indicated compounds.

Silencing was verified by Western Blot or by qRT- PCR.

Expression of Homo sapiens 14-3-3ε:

The pcDNA3.1 expression vector containing the full length human14-3-3ε sequence is from GenScript Inc., U.S.A. 24 hours before transfection, cells were plated at 50% confluency in a 6-well plate and grown overnight. 2.5 µg of plasmid DNA was diluted in Opti-MEM I Reduced Serum Media (Gibco), mixed and incubated with TransIT®-LT1 Reagent (Mirus Bio LLC) for 15 minutes at room temperature and then added dropwise to the cells. 48 hours post transfection, cells were harvested, washed with PBS and the remaining pellet was used for cytosol preparation.

For cell viability assays, 24 hours after the transfection cells were plated onto a 96-well plate (5000 cells/well) and treated the next day with indicated compounds.

RNA isolation and cDNA synthesis

The total RNA from cells was isolated using Total RNA Purification Kit (Norgen Biotek Corp.). Adherent cells were harvested from cell culture dishes by trypsinization, washed twice with PBS, the supernatant was discarded, and cells were lysed by addition of 350 µL Buffer RL. RNA was eluted with 50 µL of UltraPure™ DNase/RNase-Free Distilled Water (Invitrogen) and RNA concentration was determined by NanoDrop spectrometer.

Using 1 µg of the isolated RNA as template, cDNA was synthetized by reverse transcription using Super Script™ III Reverse Transcriptase (Invitrogen) according to manufacturers' instructions. 20 ng of cDNA from these reactions was used in qRT-PCR reactions.

qRT-PCR measurements

Obtained cDNA was analyzed in triplicate to evaluate the gene expression using SensiFAST SYBR No-ROX Kit (Bioline Reagents Ltd.). The results are normalized against hypoxanthine-guanine phosphoribosyl transferase (HPRT), the housekeeping gene.

Oligo name	Sequence
Hs_DLD_fw	GTTGAAGGAATGGCTGGTGG
Hs_DLD_rev	TGCCCAAGGATCTTCACCAT
Hs_YWHAE_fw	ACTTCCACCAACGCATCCTA
Hs_YWHAE_rev	TCACCCTGCATGTCTGAAG
Hs_HPRT_fw	CCTGGCGTCGTGATTAGTGAT
Hs_HPRT_rev	AGACGTTCAGTCCTGTCCATAA

Statistical analysis

Data are presented as mean ± SEM of n = x experiments, with x indicating the number of independent experiments performed. In general, one-way ANOVA test was performed unless stated otherwise. All statistical analyses were performed with Graph Pad Prism 7. $P<0.05$ was considered statistically significant.

6. BIBLIOGRAPHY

1. Clarke, PeterG. H. & Clarke, S. Nineteenth century research on naturally occurring cell death and related phenomena. *Anat Embryol* **193**, (1996).
2. Lockshin, R. A. & Williams, C. M. Programmed cell death—II. Endocrine potentiation of the breakdown of the intersegmental muscles of silkmoths. *Journal of Insect Physiology* **10**, 643–649 (1964).
3. Schweichel, J.-U. & Merker, H.-J. The morphology of various types of cell death in prenatal tissues. *Teratology* **7**, 253–266 (1973).
4. Galluzzi, L. *et al.* Molecular mechanisms of cell death: recommendations of the Nomenclature Committee on Cell Death 2018. *Cell Death Differ* **25**, 486–541 (2018).
5. Kerr, J. F. R., Wyllie, A. H. & Currie, A. R. Apoptosis: A Basic Biological Phenomenon with Wideranging Implications in Tissue Kinetics. *Br J Cancer* **26**, 239–257 (1972).
6. Vaux, D. L. Apoptosis Timeline. *Cell Death Differ* **9**, 349–354 (2002).
7. Yuan, J. & Horvitz, H. R. The Caenorhabditis elegans cell death gene ced-4 encodes a novel protein and is expressed during the period of extensive programmed cell death. 12.
8. Galluzzi, L. *et al.* Essential versus accessory aspects of cell death: recommendations of the NCCD 2015. *Cell Death Differ* **22**, 58–73 (2015).
9. Galluzzi, L., Bravo-San Pedro, J. M., Kepp, O. & Kroemer, G. Regulated cell death and adaptive stress responses. *Cell. Mol. Life Sci.* **73**, 2405–2410 (2016).
10. Yuan, J., Shaham, S., Ledoux, S., Ellis, H. M. & Horvitz, H. R. The C. elegans cell death gene ced-3 encodes a protein similar to mammalian interleukin-1β-converting enzyme. *Cell* **75**, 641–652 (1993).
11. Shamas-Din, A., Kale, J., Leber, B. & Andrews, D. W. Mechanisms of Action of Bcl-2 Family Proteins. *Cold Spring Harbor Perspectives in Biology* **5**, a008714–a008714 (2013).

12. Vaux, D. L., Cory, S. & Adams, J. M. Bcl-2 gene promotes haemopoietic cell survival and cooperates with c-myc to immortalize pre-B cells. *Nature* **335**, 440–442 (1988).

13. Czabotar, P. E., Lessene, G., Strasser, A. & Adams, J. M. Control of apoptosis by the BCL-2 protein family: implications for physiology and therapy. *Nat Rev Mol Cell Biol* **15**, 49–63 (2014).

14. Li, P. *et al.* Cytochrome c and dATP-Dependent Formation of Apaf-1/Caspase-9 Complex Initiates an Apoptotic Protease Cascade. *Cell* **91**, 479–489 (1997).

15. Dickens, L. S., Powley, I. R., Hughes, M. A. & MacFarlane, M. The 'complexities' of life and death: Death receptor signalling platforms. *Experimental Cell Research* **318**, 1269–1277 (2012).

16. Laster, S. M., Wood, J. G. & Gooding, L. R. Tumor necrosis factor can induce both apoptic and necrotic forms of cell lysis. 7.

17. Christofferson, D. E. & Yuan, J. Necroptosis as an alternative form of programmed cell death. *Current Opinion in Cell Biology* **22**, 263–268 (2010).

18. Vandenabeele, P., Galluzzi, L., Vanden Berghe, T. & Kroemer, G. Molecular mechanisms of necroptosis: an ordered cellular explosion. *Nat Rev Mol Cell Biol* **11**, 700–714 (2010).

19. Degterev, A. *et al.* Identification of RIP1 kinase as a specific cellular target of necrostatins. *Nat Chem Biol* **4**, 313–321 (2008).

20. Berghe, T. V., Linkermann, A., Jouan-Lanhouet, S., Walczak, H. & Vandenabeele, P. Regulated necrosis: the expanding network of non-apoptotic cell death pathways. *Nat Rev Mol Cell Biol* **15**, 135–147 (2014).

21. Weinlich, R., Oberst, A., Beere, H. M. & Green, D. R. Necroptosis in development, inflammation and disease. *Nature Reviews Molecular Cell Biology* **18**, 127 (2016).

22. Conrad, M., Angeli, J. P. F., Vandenabeele, P. & Stockwell, B. R. Regulated necrosis: disease relevance and therapeutic opportunities. *Nat Rev Drug Discov* **15**, 348–366 (2016).

23. Galluzzi, L. *et al.* Molecular definitions of cell death subroutines: recommendations of the Nomenclature Committee on Cell Death 2012. *Cell Death Differ* **19**, 107–120 (2012).

24. Yang, W. S. *et al.* Regulation of Ferroptotic Cancer Cell Death by GPX4. *Cell* **156**, 317–331 (2014).

25. Hochstein, P. & Ernster, L. Microsomal Peroxidation of Lipids and its Possible Rôle in Cellular Injury. in *Novartis Foundation Symposia* (eds. de Reuck, A. V. S. & Knight, J.) 123–135 (John Wiley & Sons, Ltd., 2008). doi:10.1002/9780470719336.ch7.

26. Yang, W. S. & Stockwell, B. R. Synthetic Lethal Screening Identifies Compounds Activating Iron-Dependent, Nonapoptotic Cell Death in Oncogenic-RAS-Harboring Cancer Cells. *Chemistry & Biology* **15**, 234–245 (2008).

27. Dixon, S. J. *et al.* Ferroptosis: An Iron-Dependent Form of Nonapoptotic Cell Death. *Cell* **149**, 1060–1072 (2012).

28. Ursini, F., Maiorino, M. & Gregolin, C. The selenoenzyme phospholipid hydroperoxide glutathione peroxidase. *Biochimica et Biophysica Acta (BBA) - General Subjects* **839**, 62–70 (1985).

29. Dolma, S., Lessnick, S. L., Hahn, W. C. & Stockwell, B. R. Identification of genotype-selective antitumor agents using synthetic lethal chemical screening in engineered human tumor cells. *Cancer Cell* **3**, 285–296 (2003).

30. Conrad, M. & Sato, H. The oxidative stress-inducible cystine/glutamate antiporter, system x c − : cystine supplier and beyond. *Amino Acids* **42**, 231–246 (2012).

31. Bröer, S. & Wagner, C. A. Structure-Function Relationships of Heterodimeric Amino Acid Transporters. *CBB* **36**, 155–168 (2002).

32. Bridges, R. J., Natale, N. R. & Patel, S. A. System xc- cystine/glutamate antiporter: an update on molecular pharmacology and roles within the CNS: System xc- cystine/glutamate antiporter. *British Journal of Pharmacology* **165**, 20–34 (2012).

33. Mandal, P. K. *et al.* System x_c^- and Thioredoxin Reductase 1 Cooperatively Rescue Glutathione Deficiency. *J. Biol. Chem.* **285**, 22244–22253 (2010).

34. Ursini, F., Maiorino, M., Valente, M., Ferri, L. & Gregolin, C. Purification from pig liver of a protein which protects liposomes and biomembranes from peroxidative degradation and exhibits glutathione peroxidase activity on phosphatidylcholine hydroperoxides. *Biochimica et Biophysica Acta (BBA) - Lipids and Lipid Metabolism* **710**, 197–211 (1982).

35. Sauzay, C. *et al.* Protein biosynthesis, a target of sorafenib, interferes with the unfolded protein response (UPR) and ferroptosis in hepatocellular carcinoma cells. *Oncotarget* **9**, (2018).

36. Larraufie, M.-H. *et al.* Incorporation of metabolically stable ketones into a small molecule probe to increase potency and water solubility. *Bioorganic & Medicinal Chemistry Letters* **25**, 4787–4792 (2015).

37. Yang, W. S. *et al.* Peroxidation of polyunsaturated fatty acids by lipoxygenases drives ferroptosis. *Proc Natl Acad Sci USA* **113**, E4966–E4975 (2016).

38. Yang, W. S. & Stockwell, B. R. Ferroptosis: Death by Lipid Peroxidation. *Trends in Cell Biology* **26**, 165–176 (2016).

39. Yin, H., Xu, L. & Porter, N. A. Free Radical Lipid Peroxidation: Mechanisms and Analysis. *Chem. Rev.* **111**, 5944–5972 (2011).

40. Maiorino, M., Conrad, M. & Ursini, F. GPx4, Lipid Peroxidation, and Cell Death: Discoveries, Rediscoveries, and Open Issues. *Antioxidants & Redox Signaling* **29**, 61–74 (2018).

41. Dixon, S. J. *et al.* Pharmacological inhibition of cystine–glutamate exchange induces endoplasmic reticulum stress and ferroptosis. *eLife* **3**, e02523 (2014).

42. Chen, Y. *et al.* Quantitative Profiling of Protein Carbonylations in Ferroptosis by an Aniline-Derived Probe. *J. Am. Chem. Soc.* **140**, 4712–4720 (2018).

43. Shah, R., Shchepinov, M. S. & Pratt, D. A. Resolving the Role of Lipoxygenases in the Initiation and Execution of Ferroptosis. *ACS Cent. Sci.* **4**, 387–396 (2018).

44. Dixon, S. J. & Stockwell, B. R. The role of iron and reactive oxygen species in cell death. *Nat Chem Biol* **10**, 9–17 (2014).

45. Seiler, A. *et al.* Glutathione Peroxidase 4 Senses and Translates Oxidative Stress into 12/15-Lipoxygenase Dependent- and AIF-Mediated Cell Death. *Cell Metabolism* **8**, 237–248 (2008).

46. Doll, S. *et al.* ACSL4 dictates ferroptosis sensitivity by shaping cellular lipid composition. *Nat Chem Biol* **13**, 91–98 (2017).

47. Yuan, H., Li, X., Zhang, X., Kang, R. & Tang, D. Identification of ACSL4 as a biomarker and contributor of ferroptosis. *Biochemical and Biophysical Research Communications* **478**, 1338–1343 (2016).

48. Conrad, M. *et al.* Regulation of lipid peroxidation and ferroptosis in diverse species. *Genes Dev.* **32**, 602–619 (2018).

49. Cichewicz, R. H. *et al.* Redox Inactivation of Human 15-Lipoxygenase by Marine-Derived Meroditerpenes and Synthetic Chromanes: Archetypes for a Unique Class of Selective and Recyclable Inhibitors. *J. Am. Chem. Soc.* **126**, 14910–14920 (2004).

50. Miotto, G. *et al.* Insight into the mechanism of ferroptosis inhibition by ferrostatin-1. *Redox Biology* 101328 (2019) doi:10.1016/j.redox.2019.101328.

51. Gao, M., Monian, P., Quadri, N., Ramasamy, R. & Jiang, X. Glutaminolysis and Transferrin Regulate Ferroptosis. *Molecular Cell* **59**, 298–308 (2015).

52. Kühn, L. C. Iron regulatory proteins and their role in controlling iron metabolism. *Metallomics* **7**, 232–243 (2015).

53. Eckenroth, B. E., Steere, A. N., Chasteen, N. D., Everse, S. J. & Mason, A. B. How the binding of human transferrin primes the transferrin receptor potentiating iron release at endosomal pH. *Proc Natl Acad Sci USA* **108**, 13089–13094 (2011).

54. Andrews, N. C. & Schmidt, P. J. Iron Homeostasis. *Annu. Rev. Physiol.* **69**, 69–85 (2007).

55. Gao, M. *et al.* Ferroptosis is an autophagic cell death process. *Cell Res* **26**, 1021–1032 (2016).

56. Kwon, M.-Y., Park, E., Lee, S.-J. & Chung, S. W. Heme oxygenase-1 accelerates erastin-induced ferroptotic cell death. *Oncotarget* **6**, (2015).

57. Hassannia, B. *et al.* Nano-targeted induction of dual ferroptotic mechanisms eradicates high-risk neuroblastoma. *Journal of Clinical Investigation* **128**, 3341–3355 (2018).

58. Hochstein, P. & Ernster, L. ADP-activated lipid peroxidation coupled to the TPNH oxidase system of microsomes. *Biochemical and Biophysical Research Communications* **12**, 388–394 (1963).

59. Kappus, H. Lipid Peroxidation: Mechanisms, Analysis, Enzymology and Biological Relevance. in *Oxidative Stress* 273–310 (Elsevier, 1985). doi:10.1016/B978-0-12-642760-8.50016-8.

60. Gibson, D. D., Hornbrook, K. R. & McCay, P. B. Glutathione-dependent inhibition of lipid peroxidation by a soluble, heat-labile factor in animal tissues. *Biochimica et Biophysica Acta (BBA) - Lipids and Lipid Metabolism* **620**, 572–582 (1980).

61. McCay, P. B., Gibson, D. D., Kuo-Lan, F. & K. Roger, H. Effect of glutathione peroxidase activity on lipid peroxidation in biological membranes. *Biochimica et Biophysica Acta (BBA) - Lipids and Lipid Metabolism* **431**, 459–468 (1976).

62. Flohé, L., Loschen, G., Günzler, W. A. & Eichele, E. Glutathione peroxidase, V. The kinetic mechanism. *Hoppe-Seyler's Z. Physiol. Chem.* **353**, 987–999 (1972).

63. Thomas, J. P., Maiorino, M., Ursini, F. & Girotti, A. W. Protective action of phospholipid hydroperoxide glutathione peroxidase against membrane-damaging lipid peroxidation. In situ reduction of phospholipid and cholesterol hydroperoxides. *J. Biol. Chem.* **265**, 454–461 (1990).

64. Gladyshev, V. N. *et al.* Selenoprotein Gene Nomenclature. *J. Biol. Chem.* **291**, 24036–24040 (2016).

65. Toppo, S., Vanin, S., Bosello, V. & Tosatto, S. C. E. Evolutionary and Structural Insights Into the Multifaceted Glutathione Peroxidase (Gpx) Superfamily. *Antioxidants & Redox Signaling* **10**, 1501–1514 (2008).

66. Martin, J. L. Thioredoxin —a fold for all reasons. *Structure* **3**, 245–250 (1995).

67. Brigelius-Flohé, R. & Maiorino, M. Glutathione peroxidases. *Biochimica et Biophysica Acta (BBA) - General Subjects* **1830**, 3289–3303 (2013).

68. Toppo, S., Flohé, L., Ursini, F., Vanin, S. & Maiorino, M. Catalytic mechanisms and specificities of glutathione peroxidases: Variations of a basic scheme. *Biochimica et Biophysica Acta (BBA) - General Subjects* **1790**, 1486–1500 (2009).

69. Orian, L. *et al.* Selenocysteine oxidation in glutathione peroxidase catalysis: an MS-supported quantum mechanics study. *Free Radical Biology and Medicine* **87**, 1–14 (2015).

70. Ingold, I. *et al.* Selenium Utilization by GPX4 Is Required to Prevent Hydroperoxide-Induced Ferroptosis. *Cell* **172**, 409-422.e21 (2018).

71. Shi, Z.-Z. *et al.* Glutathione synthesis is essential for mouse development but not for cell growth in culture. *Proceedings of the National Academy of Sciences* **97**, 5101–5106 (2000).

72. Bannai, S. & Kitamura, E. Transport Interactionof t-Cystine and L-Glutamatein Human Diploid Fibroblasts in Culture. 6.

73. Tan, S., Schubert, D. & Maher, P. Oxytosis: A novel form of programmed cell death. *Curr Top Med Chem* **1**, 497–506 (2001).

74. Lewerenz, J., Ates, G., Methner, A., Conrad, M. & Maher, P. Oxytosis/Ferroptosis—(Re-) Emerging Roles for Oxidative Stress-Dependent Non-apoptotic Cell Death in Diseases of the Central Nervous System. *Front. Neurosci.* **12**, 214 (2018).

75. Hayes, D., Wießner, M., Rauen, T. & McBean, G. J. Transport of l-[14C]cystine and l-[14C]cysteine by subtypes of high affinity glutamate transporters over-expressed in HEK cells. *Neurochemistry International* **46**, 585–594 (2005).

76. Hayano, M., Yang, W. S., Corn, C. K., Pagano, N. C. & Stockwell, B. R. Loss of cysteinyl-tRNA synthetase (CARS) induces the transsulfuration pathway and inhibits ferroptosis induced by cystine deprivation. *Cell Death Differ* **23**, 270–278 (2016).

77. McBean, G. J. The transsulfuration pathway: a source of cysteine for glutathione in astrocytes. *Amino Acids* **42**, 199–205 (2012).

78. Kobayashi, S. *et al.* Cystathionine Is a Novel Substrate of Cystine/Glutamate Transporter: IMPLICATIONS FOR IMMUNE FUNCTION. *J. Biol. Chem.* **290**, 8778–8788 (2015).

79. Erickson, A. M., Nevarea, Z., Gipp, J. J. & Mulcahy, R. T. Identification of a Variant Antioxidant Response Element in the Promoter of the Human Glutamate-Cysteine Ligase Modifier Subunit Gene: REVISION OF THE ARE CONSENSUS SEQUENCE. *J. Biol. Chem.* **277**, 30730–30737 (2002).

80. Yamamoto, M., Kensler, T. W. & Motohashi, H. The KEAP1-NRF2 System: a Thiol-Based Sensor-Effector Apparatus for Maintaining Redox Homeostasis. *Physiological Reviews* **98**, 1169–1203 (2018).

81. Banjac, A. *et al.* The cystine/cysteine cycle: a redox cycle regulating susceptibility versus resistance to cell death. 11.

82. Johnson, W. M., Wilson-Delfosse, A. L. & Mieyal, John. J. Dysregulation of Glutathione Homeostasis in Neurodegenerative Diseases. *Nutrients* **4**, 1399–1440 (2012).

83. Lewerenz, J. *et al.* The Cystine/Glutamate Antiporter System x_c^- in Health and Disease: From Molecular Mechanisms to Novel Therapeutic Opportunities. *Antioxidants & Redox Signaling* **18**, 522–555 (2013).

84. Park, H.-A. *et al.* Natural Vitamin E α-Tocotrienol Protects Against Ischemic Stroke by Induction of Multidrug Resistance-Associated Protein 1. *Stroke* **42**, 2308–2314 (2011).

85. Trompier, D. *et al.* Verapamil and Its Derivative Trigger Apoptosis through Glutathione Extrusion by Multidrug Resistance Protein MRP1. *Cancer Res* **64**, 4950–4956 (2004).

86. Franco, R. & Cidlowski, J. A. Glutathione Efflux and Cell Death. *Antioxidants & Redox Signaling* **17**, 1694–1713 (2012).

87. Skouta, R. *et al.* Ferrostatins Inhibit Oxidative Lipid Damage and Cell Death in Diverse Disease Models. *J. Am. Chem. Soc.* **136**, 4551–4556 (2014).

88. Bellinger, F. P. *et al.* Glutathione Peroxidase 4 is associated with Neuromelanin in Substantia Nigra and Dystrophic Axons in Putamen of Parkinson's brain. *Mol Neurodegeneration* **6**, 8 (2011).

89. Morris, G. *et al.* Why should neuroscientists worry about iron? The emerging role of ferroptosis in the pathophysiology of neuroprogressive diseases. *Behavioural Brain Research* **341**, 154–175 (2018).

90. Hirschhorn, T. & Stockwell, B. R. The development of the concept of ferroptosis. *Free Radical Biology and Medicine* **133**, 130–143 (2019).

91. Wang, J.-F., Shao, L., Sun, X. & Young, L. T. Increased oxidative stress in the anterior cingulate cortex of subjects with bipolar disorder and schizophrenia. *Bipolar Disorders* **11**, 523–529 (2009).

92. Medina-Hernández, V. *et al.* Increased lipid peroxidation and neuron specific enolase in treatment refractory schizophrenics. *Journal of Psychiatric Research* **41**, 652–658 (2007).

93. Yoo, M.-H. *et al.* Delineating the Role of Glutathione Peroxidase 4 in Protecting Cells Against Lipid Hydroperoxide Damage and in Alzheimer's Disease. *Antioxidants & Redox Signaling* **12**, 819–827 (2010).

94. Chen, L., Na, R., Gu, M., Richardson, A. & Ran, Q. Lipid peroxidation up-regulates BACE1 expression *in vivo* : a possible early event of amyloidogenesis in Alzheimer's disease. *Journal of Neurochemistry* **107**, 197–207 (2008).

95. Yoo, S.-E. *et al.* Gpx4 ablation in adult mice results in a lethal phenotype accompanied by neuronal loss in brain. *Free Radical Biology and Medicine* **52**, 1820–1827 (2012).

96. Wortmann, M. *et al.* Combined Deficiency in Glutathione Peroxidase 4 and Vitamin E Causes Multiorgan Thrombus Formation and Early Death in Mice. *Circ Res* **113**, 408–417 (2013).

97. Sengupta, A. *et al.* Targeted Disruption of Glutathione Peroxidase 4 in Mouse Skin Epithelial Cells Impairs Postnatal Hair Follicle Morphogenesis that Is Partially Rescued through Inhibition of COX-2. *Journal of Investigative Dermatology* **133**, 1731–1741 (2013).

98. Altamura, S. *et al.* Glutathione peroxidase 4 and vitamin E control reticulocyte maturation, stress erythropoiesis and iron homeostasis. *Haematologica* haematol.2018.212977 (2019) doi:10.3324/haematol.2018.212977.

99. Friedmann Angeli, J. P. *et al.* Inactivation of the ferroptosis regulator Gpx4 triggers acute renal failure in mice. *Nat Cell Biol* **16**, 1180–1191 (2014).

100. Matsushita, M. *et al.* T cell lipid peroxidation induces ferroptosis and prevents immunity to infection. *J Exp Med* **212**, 555–568 (2015).

101. Zhu, H., Santo, A., Jia, Z. & Li, Y. GPx4 in Bacterial Infection and Polymicrobial Sepsis: Involvement of Ferroptosis and Pyroptosis. *ROS* (2019) doi:10.20455/ros.2019.835.

102. Amaral, E. P. *et al.* A major role for ferroptosis in *Mycobacterium tuberculosis* –induced cell death and tissue necrosis. *J. Exp. Med.* **216**, 556–570 (2019).

103. Yamane, D. *et al.* Regulation of the hepatitis C virus RNA replicase by endogenous lipid peroxidation. *Nat Med* **20**, 927–935 (2014).

104. Jung, M., Mertens, C., Tomat, E. & Brüne, B. Iron as a Central Player and Promising Target in Cancer Progression. *IJMS* **20**, 273 (2019).

105. Toyokuni, S. Role of iron in carcinogenesis: Cancer as a ferrotoxic disease. *Cancer Science* **100**, 9–16 (2009).

106. Wu, J. *et al.* Intercellular interaction dictates cancer cell ferroptosis via NF2–YAP signalling. *Nature* **572**, 402–406 (2019).

107. Jiang, L. *et al.* Ferroptosis as a p53-mediated activity during tumour suppression. *Nature* **520**, 57–62 (2015).

108. Tarangelo, A. *et al.* p53 Suppresses Metabolic Stress-Induced Ferroptosis in Cancer Cells. *Cell Reports* **22**, 569–575 (2018).

109. Aikens, J. & Dix, T. A. Perhydroxyl Radical (HOO') Initiated Lipid Peroxidation. *The Journal of Biological Chemistry* **266**, 15091–15098 (1991).

110. Murphy, M. P. How mitochondria produce reactive oxygen species. *Biochem. J.* **417**, 1–13 (2009).

111. Bunik, V. I. Redox-Driven Signaling: 2-Oxo Acid Dehydrogenase Complexes as Sensors and Transmitters of Metabolic Imbalance. *Antioxidants & Redox Signaling* **30**, 1911–1947 (2019).

112. Bunik, V. I. & Sievers, C. Inactivation of the 2-oxo acid dehydrogenase complexes upon generation of intrinsic radical species: Radicals upon oxidation of 2-oxo acids. *European Journal of Biochemistry* **269**, 5004–5015 (2002).

113. Li, N. *et al.* Mitochondrial Complex I Inhibitor Rotenone Induces Apoptosis through Enhancing Mitochondrial Reactive Oxygen Species Production. *J. Biol. Chem.* **278**, 8516–8525 (2003).

114. Sullivan, L. B. *et al.* Supporting Aspartate Biosynthesis Is an Essential Function of Respiration in Proliferating Cells. *Cell* **162**, 552–563 (2015).

115. King, M. & Attardi, G. Human cells lacking mtDNA: repopulation with exogenous mitochondria by complementation. *Science* **246**, 500–503 (1989).

116. Weïwer, M. *et al.* Development of small-molecule probes that selectively kill cells induced to express mutant RAS. *Bioorganic & Medicinal Chemistry Letters* **22**, 1822–1826 (2012).

117. Shimada, K. *et al.* Global survey of cell death mechanisms reveals metabolic regulation of ferroptosis. *Nat Chem Biol* **12**, 497–503 (2016).

118. Gaschler, M. M. *et al.* FINO2 initiates ferroptosis through GPX4 inactivation and iron oxidation. *Nat Chem Biol* **14**, 507–515 (2018).

119. Vučković, A. *et al.* Inactivation of the glutathione peroxidase GPx4 by the ferroptosis-inducing molecule RSL3 requires the adaptor protein 14-3-3ε. *FEBS Lett* 1873-3468.13631 (2019) doi:10.1002/1873-3468.13631.

120. Ernster, L. Oxygen as an environmental poison. *Chemica Scripta* 525–534 (1986).

121. Gascón, S. *et al.* Identification and Successful Negotiation of a Metabolic Checkpoint in Direct Neuronal Reprogramming. *Cell Stem Cell* **18**, 396–409 (2016).